2021

Review on machining of additively manufactured nickel and titanium alloys

Navneet Khanna

Kishan Zadafiya

Tej Patel

Yusuf Kaynak

Rizwan Abdul

See next page for additional authors

10.1016/j.jmrt.2021.09.088 Khanna, N., Zadafiya, K., Patel, T., Kaynak, Y., Rashid, R. A. R., & Vafadar, A. (2021). Review on machining of additively manufactured Nickel and Titanium alloys. *Journal of Materials Research and Technology*, *15*, 3192-3221. https://doi.org/10.1016/j.jmrt.2021.09.088

Authors

Navneet Khanna, Kishan Zadafiya, Tej Patel, Yusuf Kaynak, Rizwan Abdul, Rahman Rashid, and Ana Vafadar

Available online at www.sciencedirect.com

jmr&t Journal of Materials Research and Technology

journal homepage: www.elsevier.com/locate/jmrt

Review Article

Review on machining of additively manufactured nickel and titanium alloys

Navneet Khanna [a,**], *Kishan Zadafiya* [a], *Tej Patel* [a], *Yusuf Kaynak* [b], *Rizwan Abdul Rahman Rashid* [c], *Ana Vafadar* [d,*]

[a] *Advanced Manufacturing Laboratory, Institute of Infrastructure Technology Research and Management (IITRAM), Ahmedabad, 380026, India*

[b] *Department of Mechanical Engineering, Marmara University, Goztepe Campus, 34722, Kadikoy, Istanbul, Turkey*

[c] *School of Engineering, Swinburne University of Technology, Hawthorn, Victoria, 3122, Australia*

[d] *School of Engineering, Edith Cowan University (ECU), Joondalup, 6027, Western Australia, Australia*

ARTICLE INFO

Article history:
Received 19 August 2021
Accepted 20 September 2021
Available online 29 September 2021

Keywords:
Machining
Additive manufacturing
Nickel alloy
Titanium alloys
Tool wear analysis
Surface integrity analysis

ABSTRACT

The machining of nickel and titanium-based superalloy components is very expensive and involves unusually high lead times compared with other engineering metals such as steels and aluminum. This has led to the development of most suitable additive manufacturing (AM) processes to fabricate these difficult-to-machine metals into near-net shape parts, thereby reducing the lead time and material waste, and significantly increasing productivity. Nonetheless, finish machining is still required on the AMed metal components to meet the dimensional and surface requirements of the application. Several research studies have investigated the machinability of AMed nickel and titanium alloy workpieces and have compared the results with the machining responses of wrought counterparts, which is detailed in this review. The categorization of the literature is based on the machining operations including turning, milling, drilling, and non-conventional machining, and the observations are discussed in accordance with various input parameters such as workpiece characteristics (hardness, microstructures) and anisotropy in mechanical properties due to build orientations during the AM process. Moreover, the influence of these parameters on cutting forces and temperatures, chip formation, and tool wear is analyzed and reported. From this review, it is found that the machinability of AMed nickel and titanium workpieces is quite different to the machining responses of their wrought counterparts. Further thorough experimentation is required to develop optimized machining parameters for AMed metal parts, while an exploration of different cutting tool geometries, coolant, and lubrication strategies for enhanced tool performance for machining AMed workpieces is essential. Finally, this study reviews the state of contemporary research, and offers suggestions for future research.

* Corresponding author.
** Corresponding author.
E-mail addresses: navneetkhanna@iitram.ac.in (N. Khanna), a.vafadarshamasbi@ecu.edu.au (A. Vafadar).

https://doi.org/10.1016/j.jmrt.2021.09.088

Nomenclature

AM	Additive Manufacturing
AMed	Additively manufactured/fabricated
CAD	Computer-Aided Design
SLA	Stereolithography
FDM	Fused Deposition Modeling
SLS	Selective Laser Sintering
LC	Laser Consolidation
3DP	Three-Dimensional Printing
LOM	Laminated Object Manufacturing
GMAW	Gas Metal Arc Welding
GTAW	Gas Tungsten Arc Welding
DMLS	Direct Metal Laser Sintering
LAM	Laser Additively Manufactured
LPBF	Laser Powder Bed Fusion
SLM	Selective Laser Melting
EDM	Electrical Discharge Machining
MQL	Minimum Quantity Lubrication
EMQL	Electrostatic Minimum Quantity Lubrication
EBM	Electron Beam Melting
WAAM	Wire Arc Additive Manufacturing
PAW	Plasma Arc Welding
DMD	Direct Metal Deposition
LENS	Laser Engineered Net Shaping
LMD	Laser Metal Deposition
DED	Directed Energy Deposition
N	Spindle speed in RPM
V_c	Cutting speed
F	Feed rate
a_p	Depth of cut

1. Introduction

Additive manufacturing (AM) originated in 1987 when Chuck Hull introduced the first industrially available stereolithography machine. The only shortcoming of this technology was capable to produce only plastic 3D printed parts. In 1994, EOS introduced the first metal 3D printer, EOSINT M250, which used Direct Metal Laser Sintering (DMLS) technology to print metallic parts. In general, AM uses 3D CAD models to produce the end products layer by layer [1], which is in contrast to subtractive methods like turning and milling, which involve removing material to produce the end products. In the past three decades, metal AM has taken a big leap and it can be classified into three categories; (I) according to the material used for AM [2], (II) direct and indirect processes based on bonding method and (III) as per the state of input material [3–5]. On the grounds of bonding methods, AM can be classified as (i) powder bed fusion, (ii) direct energy deposition, (iii) binder jetting, (iv) material extrusion, (v) VAT photopolymerization, (vi) material jetting, and (vii) sheet lamination by ASTM international [6]. (i), (ii), (iii) can be used for printing powders, (iv) can be used for printing filaments, (v), (vi) can be used for printing liquids and (vii) can be used for printing solid layers. The flowchart in Fig. 1 shows the grouping of AM operations on the basis of the condition of raw material [7].

AM processes as a whole are developed to produce complex objects, which are difficult or impossible to manufacture through conventional machining processes. Moreover, AM processes being cost-effective and are viable for producing small batches [8]. In the stereolithography (SLA) process, liquid photosensitive resin is transmuted to solid matter using selective resin vat exposure to ultraviolet light [9]. During Fused Deposition Modeling (FDM) polymer is passed through a heated liquefier, which is then ejected from a minute nozzle to build a 3D object onto a building platform [10]. Selective Laser Sintering (SLS) fuses metal alloy powder particles using a laser beam on the powder bed, layer by layer, to achieve pre-defined CAD object [11,12]. Selective Laser Melting (SLM) is an extension of the SLS process, wherein high-power laser melts the metal alloy powders on the powder bed and forms dense predefined metal object [13,14]. Electron Beam Melting (EBM) is akin to SLM the only difference being that this AM technique utilizes an electron beam in a vacuum environment rather than employing a laser beam. EBM can build void-free, dense, and strong components [15]. Direct Metal Deposition (DMD) (known by various names; Laser Cladding, Laser Metal Deposition (LMD), Laser Consolidation (LC), Direct Energy Deposition (DED), or Laser Engineered Net Shaping (LENS) [3,7,16]) fully melts the metal alloy powders by employing a laser beam. The powder is supplied by a nearby feeding nozzle (off-axial or coaxial). DMD process is capable of constructing very thin walls due to the minute heat effect zone [17]. This technology is used as both an AM process as well as a surface modification technology for repair applications [18].

Three-Dimensional Printing (3DP) employs an ink-jet printing head to sprinkle the liquid binder onto the thin layer of powder lying on the powder bed. The piston clutching the component sink one layer and one-layer powder is put in again and the process is repeated until the part is completed [19]. Laminated Object Manufacturing (LOM) uses heat-sensitive adhesive surfaced metal sheets, laser, roller, and moving bed. The CAD model is sliced into thin cross-sections. The laser is fixed above a moving bed on which the sheet is fixed, the bed moves in the manner predefined by the CAD model aiding the laser to cut counters of the component's geometry. The cutout layers unite when a hot roller compresses them [20]. Lastly, wire-based AM processes are developed specifically for metal alloys, for which researchers utilize Gas Metal Arc Welding (GMAW), Plasma Arc Welding (PAW), and Gas Tungsten Arc Welding (GTAW) [21]. These wire-based AM processes use metal alloy wire as feedstock and are open atmosphere processes and thus do not involve a vacuum or inert gas compartment. This fact aids these processes to manufacture parts without the size limitation; large parts of aerospace industries can be manufactured cost-effectively by these methods [21–23]. However, GTAW has superiority over GMAW in terms of independent control over deposition rate and heat input [24]. The latest technology in this category of AM is Wire + Arc Additive Manufacturing (WAAM), which is a low investment extension of GTAW [19]. WAAM also uses electric arc as heat source and filler metal alloy wire as feedstock [25,26]. WAAM employs a GTAW torch head controlled by a CNC machine along with an automatic wire feeding nozzle connected adjacent to the head, this system utilizes a metal alloy base plate identical to feedstock

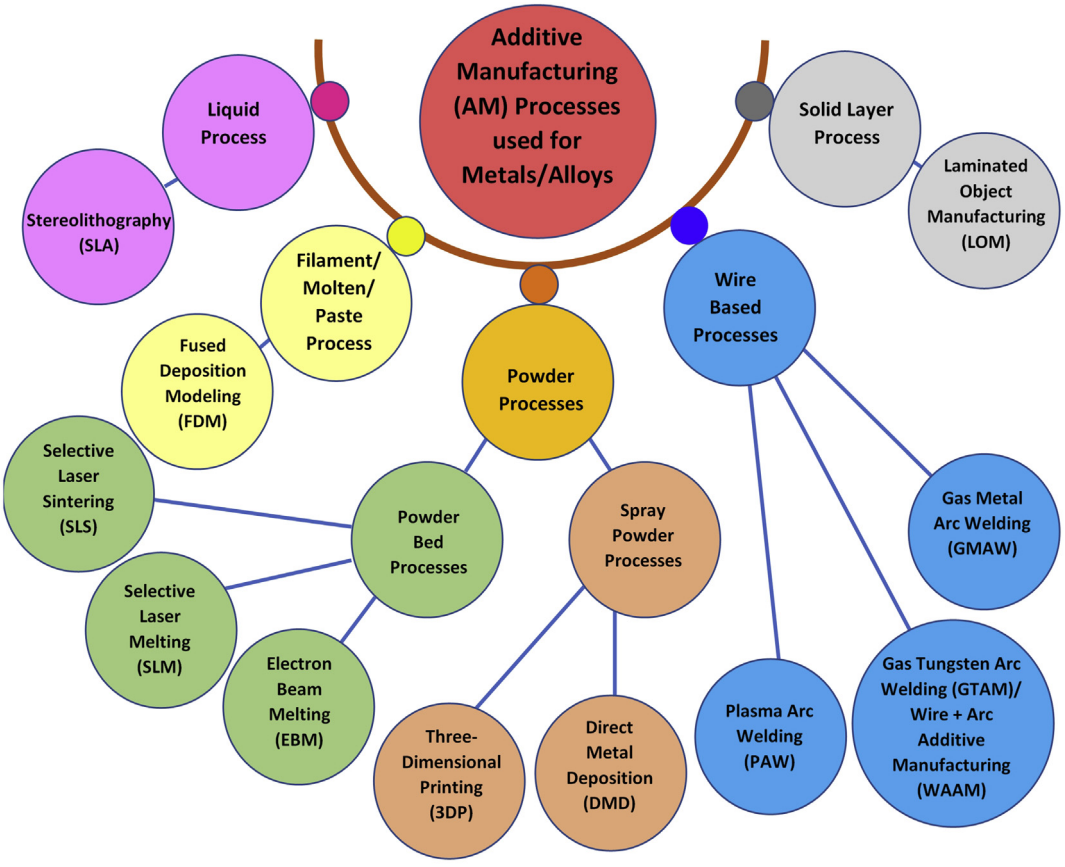

Fig. 1 – Classification of AM processes used to fabricate the metal components [7,21].

in composition [27]. By using WAAM near-net parts are obtained [6], and manufacturers can skip expensive rough finish machining and can directly leap to finishing operations [24,25]. Another process under this category is based on friction stir welding; termed as Friction Stir Additive Manufacturing (FSAM) [4], is a newly developed and commercially made available by MELD manufacturing [28].

Since the last decade, Hybrid Additive Manufacturing (HAM) processes are developed to enhance the previously available AM processes. Employing HAM will allow engineers to benefit from the advantages of two or more different processes within the same work chamber. Utilizing HAM will help manufacturers to produce components in reduced time or with superior quality [29,30]. Hybrid manufacturing proposes that HAM will always yield a grander outcome when contrasted to the sum of separate processes [31]. HAM generally utilizes a single AM process with surface enhancement or finish-machining processes, secondary processes, to improve the metrological accuracy, surface enhancement, microstructure, and physical properties augmentation of the additively manufactured components. HAM can employ any of turning, grinding, milling, drilling, re-melting, ablation, burnishing, pulsed laser deposition, and many more as secondary processes [4,32].

AM has applications in almost every industry. The aerospace industry is one of the largest industries where AM is employed. The AM process can manufacture full-scale components as well as replacement parts with superior quality, less material usage, and economically [7]. Components with complex shapes, large sizes, and advanced materials can be easily manufactured using AM for aerospace and defense sectors [33]. Further, automotive, biomedical and dental, tooling, nano-manufacturing, railway, construction and building, Electronic and communication, Mining, energy industries, and others rely heavily on AM processes in present times [34–40]. Among the AMed alloys, the nickel and titanium-based alloys are widely used in different industries.

Nickel-based superalloys possess second place for research studies after titanium alloys in the AM field. AM helps to overcome the high manufacturing cost and characteristics of higher strength at a preeminent temperature of conventionally produced nickel-based superalloys. Nickel-based superalloys exhibit higher creep resistance and higher strength at a high temperature which makes them more exceptional materials for aerospace, marine, aeronautical and chemical industries. There are many nickel-based superalloys consists of several categorizes of Inconel such as Inconel 625, Inconel 718, Inconel 939, etc. [41]. Inconel 718 has been used in different industrial applications such as gas turbine engines and general electric aviation components to provide critical functionality as Inconel 718 exhibited higher mechanical stability up to 650 °C, creep resistance, and higher strength. On the other hand, the poor machinability and the self-hardening characteristic of Inconel 718 significantly increases the cutting force and consequently reduces the tool life [42,43]. Allegheny Technologies Incorporated (ATI) 718 PLUS is a new

class of AMed nickel-based superalloy, which exhibits better properties at higher temperature and good fabricability. This ATI 718 PLUS material has better thermal stability than Waspaloy with retentive process characteristics of Inconel 718 alloy [44,45]. Inconel 625 is hard to shape by conventional methods. The design flexibility of AM provides an opportunity to produce the parts of Inconel 625 containing complex shapes. Furthermore, the finishing process can notably enhance the surface quality of the final product [46].

AMed titanium alloys are extremely feasible for every industry owing to their better mechanical and corrosion properties. Traditional manufacturing process poses higher overall cost for the part due to wastage of material, high affinity to the tool, low thermal conductivity, thus titanium alloys are placed in the first place by the research community in AM field. Ti–6Al–4V is specifically the number one titanium alloy in AM field [47–49]. Ductility, low density, high specific strength, and biocompatibility, confrontation to fatigue fracture, corrosion, and high-temperature properties of Ti–6Al–4V, an $\alpha + \beta$ titanium alloy, allow it to be widely used in the aerospace industry in jet engines, turbines, and airframe as a result of its high strength to weight ratio [50,51]. It is also widely used in automobile, biomedical, energy, chemical, and marine sectors. Many complicated shapes of components can be easily manufactured for this hard-to-machine alloy and are ready to use in low lead time. Generally, SLM, DMD, and EBM processes are used to AMed Ti–6Al–4V [48]. This article focuses on the machinability (conventional and nonconventional) of AMed nickel and titanium alloys.

2. Bifurcation of literature survey

This section of the review briefly encapsulates the bifurcation of the literature survey. A total of 54 published papers on machining have been considered to bifurcate the literature survey. Fig. 2(a) shows the bifurcation of research according to the machining processes while Fig. 2(b–d) bifurcate the literature survey as per continents, type of material, and additive manufacturing processes, respectively. From Fig. 2(a), it can be seen that limited studies have been carried out on the nonconventional machining of AMed material followed by the drilling process. Fig. 2(b) bifurcates the research studies that have been conducted in the field of machining of AMed

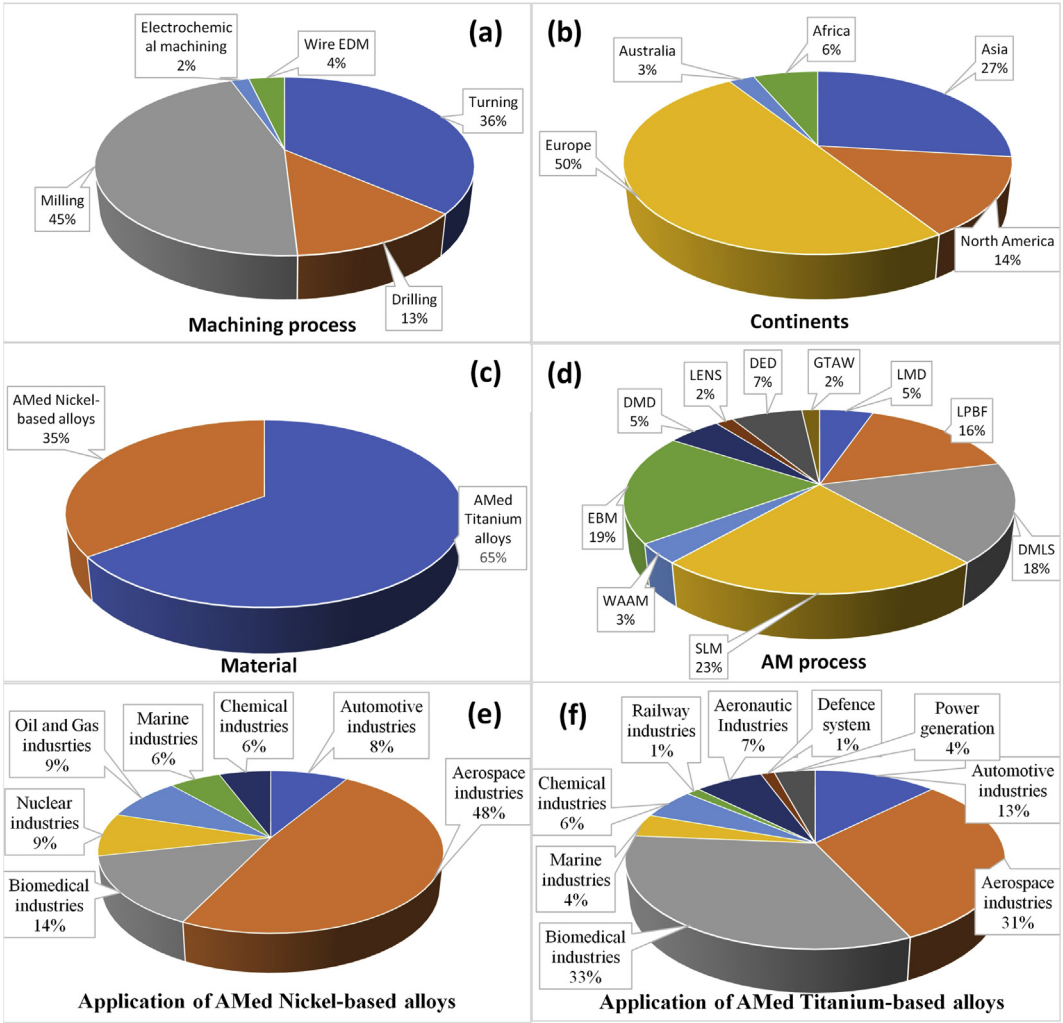

Fig. 2 – Bifurcation of literature survey according to the (a) machining process, (b) continents, (c) Material, (d) AM processes, (e) application of AMed nickel-based alloys, and (f) application of AMed nickel-based alloys.

material as per the continents. Some continents like Africa and Australia followed by North America are recognized where few studies have been done for machining of AMed materials. The machining and the characterization of the AMed material is the most advanced field of the manufacturing sector. This comparison allows us to identify the continents according to industrial advancement especially in the field of machinability of AMed parts. Fig. 2(c) reveals that many researchers have been analyzed the machining performance of AMed titanium alloys. However, few studies are available that focuses on the machinability of AMed Nickel-based alloys such as Inconel 625, Inconel 718, Inconel 939, etc. As shown in Fig. 2(d), many AMed materials are fabricated using SLM followed by EBM while fewer studies considered the AMed material produced by LENS. Fig. 2(e) and (f) shows the bifurcation according to the industrial application of nickel and titanium-based alloys, respectively. Nickel-based alloys exhibited the majority of their application in aerospace industries while titanium-based alloys are wildly used in biomedical industries followed by aerospace industries.

Fig. 3 presents the comparison among the cutting environment used in machining of AMed materials for both titanium and nickel-based alloys. The majority of the research studies have explored the machinability of AMed materials under dry machining conditions. Minimum quantity lubrication (MQL) possesses better lubrication characteristics with environmental friendliness. However, limited machining of AMed material has been done using the MQL strategy. There was no research study on the effect of cryogenic cooling on the machining behavior of AMed nickel and/or titanium-based alloys.

Fig. 4 shows the correlation between the measured output responses when machining AMed nickel and titanium-based alloys. Several papers show the conclusion of machining parameters, cutting environments, and AM processes on the surface roughness, microstructure, tool wear, cutting force, surface integrity, and chip morphology. However, there are few studies available that show the effect of AM processes and machining environment on the fatigue fracture of a workpiece, tool breakage, machining induced hardness, and cutting temperature.

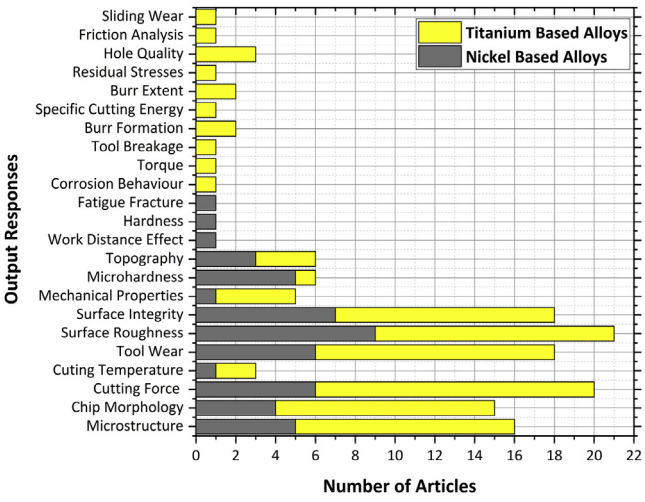

Fig. 4 – A histogram showing the comparison between the measured output responses when studying machineabilities of AMed nickel and titanium-based alloys.

Fig. 5 shows the comparison among the types of tools that were used in machining of AMed titanium and nickel-based alloy. A histogram clearly reveals that the coated tools were widely used during the different machining processes for both nickel and titanium-based alloys. However, there are very few studies available that investigated the effect of ceramic tools on the machining performance of AMed titanium-based alloys. Besides, there was no experimental work done that identifies the influence of ceramic tools when machining AMed nickel-based alloys.

Fig. 6 renders the number of publications published in recent years. This bifurcation contains only the papers of machining of AMed nickel and titanium-based alloys.

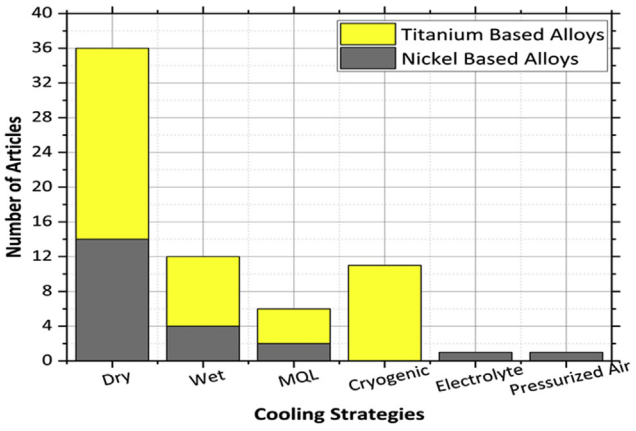

Fig. 3 – A histogram showing the bifurcation of literature survey among the cutting environments.

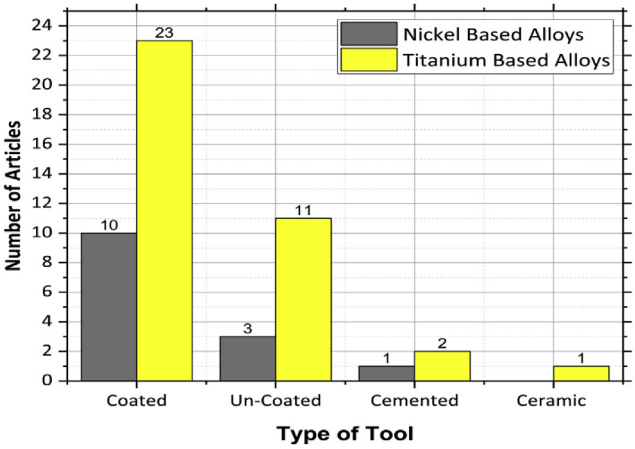

Fig. 5 – A comparison showing the used cutting tools during the machining of AMed nickel and titanium-based alloys.

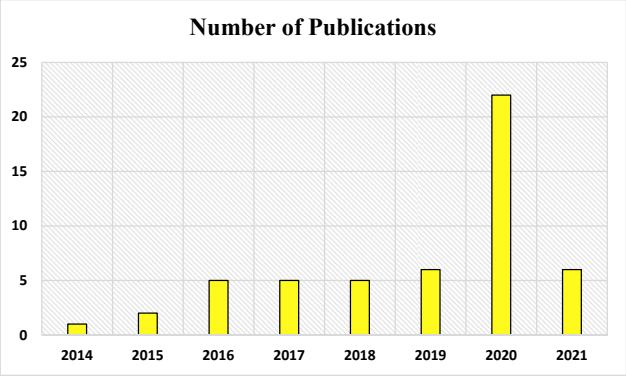

Fig. 6 – Numbers of publications published in the recent years on the machining of AMed nickel and titanium-based alloys.

3. Machining of AMed nickel-based alloys

3.1. *Conventional machining*

3.1.1. *Turning process*

The turning process is one of the commonly used conventional manufacturing systems in industry and academia. Also, the literature survey shows that this process is considered as a finishing post-process for the nickel-based alloy AMed parts. Chen et al. [52] performed the turning of LAMed Inconel 718 to investigate machinability. The LAMed Inconel 718 exhibited higher thermal conductivity, lower density, heterogeneous microstructure, and minor microhardness compared with the wrought Inconel 718. The LAMed workpiece possessed uneven and rough surface roughness. The microstructure of LAMed Inconel 718 was fine equiaxed crystals in building direction and columnar in subsurface area. The main reason for irregular microstructure was grain epitaxial growth which occurred due to the molten pools heat dissipation along to the building direction. The dense microstructure of wrought superalloy resulted in a higher density of wrought workpiece compared to LAMed workpiece. The smaller microhardness, lower cutting temperature due to the higher thermal conductivity, and poor density resulted in the generation of non-uniform chips with irrepressible outflow and serrated edge. A reduction in cutting vibration, cutting force, and machining temperature of 16.67%, 9.67%, and 6.29%, respectively, was noted with coated carbide cutting tools compared with the wrought Inconel 718. The coated carbide tool exhibited better machining performance than cemented carbide tool. The cutting temperature and the cutting force were lowered by 7.04% and 29.78% with coated carbide tool than cemented carbide tool. Furthermore, the coated carbide tool increased the tool life by about 5 times compared with the cemented tool.

3.1.2. *Milling process*

The milling operation is also used as a finish-machining process to achieve the dimensional accuracy and anticipated surface roughness of the AMed component. Besides, the fabrication of complex shapes of the AMed part can be possible with the finish-milling process. The machinability of the AMed Inconel 718 with and without post heat treatment was studied during the turning and milling processes [56]. In this study, the higher machining force was obtained with laser cladding workpiece with heat treatment compared with the non-heat-treated workpiece and base material for both turning and milling processes. The material with laser cladding showed a lower cutting force value compared with non-heat-treated material. The reduction of the cutting coefficient led to better machinability of the laser cladding workpiece. However, the heat treatment had no remarkable effect on the surface roughness. Yang et al. [57] studied the surface characteristics and the surface topography during the milling of AMed Inconel 625 by LMD. The surface quality was significantly reduced by the presence of adhered and smeared material particles. The occurrence of jagged feed marks with gas pores was also noted. The orientation of the cutting tool concerning the build direction had a major impact on the surface quality of the ultimate machined components. The study also revealed that when the build direction was perpendicular to the cutter feed, lower surface defects were found. The fracture marks, cracks, gas pores, and segmentations of saw-tooth chips were observed during chip morphology investigation. All these surface defects could not be eliminated continuously; however, they could be lowered by the use of optimal machining parameters.

In another study, Jarosz et al. [58] proposed a machining force model to foresee the cutting force when performing face milling operation for Inconel 625 additively fabricated parts using LPBF technology. It was observed that the feed rate, cutting speed, and workpiece-cutter orientation had remarkable impacts on the cutting force. The influence of the feed/tooth was also noted to be significant depending on the cutter orientation and applied cutting speeds. Besides, the machinability of the AMed Inconel 625 was affected by the cutter orientation and the scan strategy rotation. A maximum error of 2.69% was found compared to the model verification data and the experimental data of the cross-sectional area of chips to verify the accuracy of the proposed force model.

Sen et al. [59] worked on the effect of milling operations of the AMed Inconel 939 parts fabricated by DMLS. The results showed that the direction of the cutter relative to the direction of the build had an insignificant effect on the surface roughness of the machined part. The surface roughness increased with growing cutting speed and feed which exhibited an adverse correlation between productivity and surface integrity for AMed Inconel 939. In addition, a higher hardness was observed with machined Inconel 939 surface compared with the selective laser melted condition. It was observed that the heat-treated Inconel sample had higher hardness and lower surface value compared with as-built.

Fei et al. [60] examined the impact of the machining parameters on the AMed Inconel 625 parts fabricated by LPBF during the finish milling process. The increasing chip load with rising feed and cutting speed resulted in the increment of milling load. The milling force was significantly influenced by the cutting direction normal to the build direction. The machinability of the material was highly dependent on the build direction. This can be attributed to the fact that the microstructure and the physical properties of the AMed

material were reliant on the build direction and hence the effect of build direction on the milling forces was uncertain.

In another study, Fei et al. [61] examined the cutting force during the face milling of AMed Inconel 625 via LPBF with different cutting orientations. The impact of the layer scan strategy rotation and cutting direction on the cutting force was briefly evaluated. The feeding along with the direction of columnar grain growth had a peak value of cutting force while the cutting along or normal to the build direction had a major impact on the milling force. The microstructure and the physical parameters were significantly affected by the scanning strategy and thus the scanning strategy had a remarkable influence on the milling force. The generated chips were fan-shaped and discontinuous. Also, cracks were generated along the radial direction on the inner side of the chips.

The optimum machining parameters were investigated by Periane et al. [62] for face milling of additively and conventionally manufactured Inconel 718 parts. The conventionally manufactured Inconel part was fabricated by the cast and wrought process, while the SLM method was used as AM. The AMed Inconel was further subjected to the Aeronautic heat treatment (AHT) and Hot isostatic pressing (HIP) to attain the same hardness and tensile properties as that of the cast and wrought parts. The findings exhibited that the specific cutting energy for MQL and dry was nearly the same. The MQL lowered the energy consumption of the AMed sample by 15% and 27% compared with wet and dry machining environments, respectively. Lower surface roughness was achieved using a 0.05 mm feed rate and 20 m/min cutting speed with the MQL coolant. However, the surface roughness for the AMed sample under the emulsion environment was observed to be high at higher machining conditions compared with the surface roughness of the cast and wrought samples. The overall results for lower surface modification and reduced energy consumption were obtained with the emulsion cutting strategy compared with MQL and dry conditions. The existence of the δ phase in the cast and wrought sample led to higher tool wear compared with the AMed sample. The 20 m/min of cutting speed and feed of 0.05–0.075 mm/tooth were optimized for cast and wrought sample, while for the AMed Inconel 718, the cutting speed and feed rate of 20–30 m/min and 0.05–0.15 mm/tooth was optimized, respectively. For both fabricated parts, the machining parameters criteria were selected based on the achieved minimum surface roughness and lower power consumption.

Tascioglu et al. [63] analyzed the wear resistance property and surface quality of Inconel 625 produced by SLM during the finish milling operation. The findings revealed that the post-machining process such as finish machining could reduce the wear rate by 50% and enhance the surface quality. The feed rate was the influential parameter that affected wear resistance and surface quality. Also, the lower feed rate could improve the surface quality. Furthermore, the higher feed rate led to an increment in wear characteristics and hardness.

Ostra et al. [64] examined the cutting force and chip morphology during the milling of AMed Inconel 718 fabricated by LMD. The tensile and yield strength values of AMed Inconel were almost comparable with forged Inconel workpieces. The forged workpiece showed a higher elongation at fracture compared with the AMed Inconel workpiece. This higher elongation characteristic of a forged workpiece at fracture generated a spiral-shaped chip while straight and shorter chips were obtained while machining the AMed workpiece.

Ji et al. [65] studied the machinability and microstructure of the AMed Inconel 718 produced by SLM during the micro-milling process. The induced thermal and the plastic deformation due to the relative equilibrium resulted in recrystallization and refinement of the grain, respectively, during machining of Inconel 718. The results showed that the compressive residual stresses in the SLMed component were lower than that of the wrought component. This is due to the cutting force and the condition of the thermal loading. Furthermore, the tool wear was observed to be lower in the machining of the SLM component compared with the wrought component when the feed rate and cutting speed were increased. This is because of the lower hardness values of SLMed Inconel 718 compared with the wrought Inconel 718. In this study, the lower surface roughness was also examined while the inspection of the SLMed component because of the lower burr formation and tool wear. The feed rate followed by the spindle speed has a higher influence on the surface roughness (as shown in Fig. 7). The contact between the workpiece and tool could be lower by the increasing feed rate, which enhances the surface finish at a higher feed rate. The precipitation hardening characteristic and the lower cutting temperature of the SLM fabricated component were the responsible parameters for the lower hardness in contrast with the wrought component.

3.1.3. *Drilling process*

To drill a hole in AMed metal alloys with proper dimensional accuracy is one of the major challenges faced by industries. Karabulut and Kaynak [69] explored the machinability of the AMed Inconel 718 fabricated by SLM in terms of hole quality, microstructure, surface topography, and subsurface and surface microhardness when drilling. The surface quality of the AMed Inconel 718 was significantly enhanced by the drilling process. The work hardening defect induced by increasing

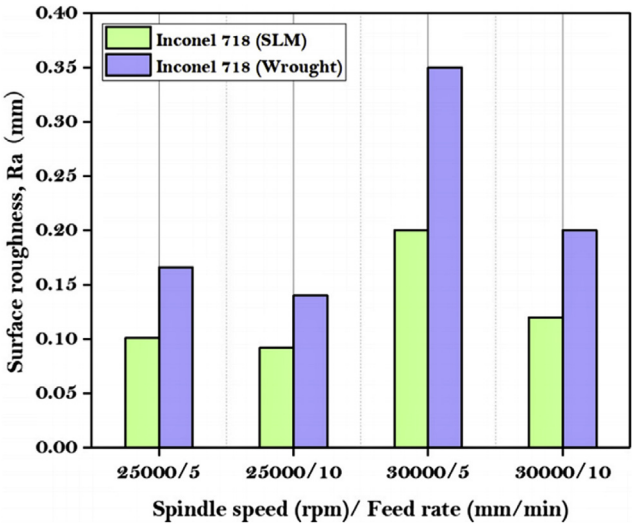

Fig. 7 – The variation in the surface roughness at various feed rates and spindle speed [65].

feed rate significantly increased the subsurface and surface microhardness.

3.2. Non-conventional machining

3.2.1. Electrochemical process

Electrochemical machining is one of the major electro-machining processes which allows better accuracy to produce 3-D complicated shaped components of hard-to-cut metal alloys. Lynch et al. [70] proposed COOLPULSE the surface finishing strategy for AMed Inconel 718 fabricated by LPBF with electrochemical machining. The cathode tooling and the material lattice coupons have been fabricated and designed. The tooling design contained pots that properly circulated the electrolyte within and around the Inconel 718 lattice coupons. Further, the design inspection exhibited better removal of material from the external and internal workpiece surface. The enhanced surface topography and 70% of reduction in surface roughness for the internal surface were observed with white light interferometry. The measuring parameters such as the thickness of the ligament and roughness depth profiling revealed that the lattice surface roughness of the core was also improved. The proposed method has successfully mitigated the reduction of the surface fatigue life of AMed lattices.

3.2.2. Wire-EDM process

Wire-EDM is an important non-conventional machining process that allows high-precision and high-speed machining with excellent dimensional precision. Ozaner et al. [71] studied the impact of machining parameters on mechanical characteristics and surface integrity during the wire EDM of AMed Inconel 939. The study revealed that the voltage, pulse on, and pulse off have significantly affected the surface texture and thus the mechanical characteristics. The effect plots divulged that the surface roughness and the recast layer were highly influenced by the pulse on time. The increasing pulse in time increased the surface roughness and the recast layer. The recast growth was influenced by the ratio of pulse off to pulse on, exhibited in Fig. 8, the recast layer thickness was reduced with increasing pulse off to pulse on ratio. The sudden increment in surface roughness was observed with increasing recast layer thickness and the roughed surface lowered the tensile strength at a higher voltage. The formation of elongated grains during manufacturing generated the anisotropy in mechanical characteristics and microstructure and hence the variation in the tensile strength was noted with different building directions. The material removal took place at high discharge energy produced larger craters. However, the pulse off had an inverse relation with surface roughness. This could be attributed to the fact that the decreasing recast layer reduced the crater depth and the flushing occurred during the additional time provided at high pulse off.

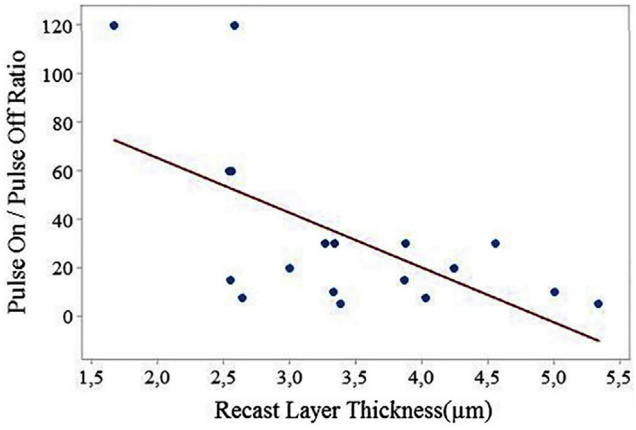

Fig. 8 – Effect of pulse off/pulse on ratio on the thickness of Recast layer [71].

3.3. Summary

From the literature survey in sections 3.1 and 3.2, it was found that the AMed materials possess higher hardness compared with the conventional material which increases the cutting force and tool wear during machining. Nonetheless, the post-machining processes proved prolific to improve the machined surface roughness with increased tool life in several cases. Additionally, many research studies exemplify the effect of different cooling strategies such as dry, wet, emulsion, and MQL on the machinability of the AMed nickel-based alloys; however, the effect of cryogenic cooling and nano-lubrication has not been explored in any research study. The synopsis of the literature review is exhibited in Table 1.

4. Machining of additively manufactured titanium-based alloys

4.1. Conventional machining

4.1.1. Turning process

Turning is a commonly used finish machining process to obtain the rotatory components. Polishetty et al. [72] evaluated the outcomes of machining parameters on the cutting force and surface roughness when turning the wrought and AMed Ti–6Al–4V produced by SLM. The cutting force was remarkably influenced by the hardness and the yield strength of the AMed material. Higher cutting force was observed with AMed titanium alloy compared with the wrought. The higher hardness of the AMed alloys could resist the breakage which required more effort to remove the chips and hence the cutting force increased. The tool wear had a higher impact on the cutting force when turning of AMed Ti–6Al–4V whereas thermal softening had played an important role while machining of wrought Ti–6Al–4V. An increase in cutting speed increased the cutting forces during machining of AMed material while inverse relation between cutting force and cutting speed was noted while turning of wrought material. The AMed titanium exhibited lower surface roughness compared with the wrought titanium due to the brittle characteristic and higher hardness of the AMed titanium alloy. The thermal softening effect and machining vibration resulted in higher surface roughness with an increasing feed rate. At the higher cutting speed, the thermal softening reduced the quantity of adhered material and the formation of build-up edge lowered the surface roughness.

Table 1 – Summary of literature review for non-conventional machining of AMed nickel-based alloy.

Ref No.	Machining process	Workpiece material	AM process	Cooling/ Lubrication strategy	Machining parameters	Investigated machining responses
[52]	Turning	Inconel 718	DLMS	Dry	V_c – 60 m/min a_p – 0.4 mm F – 0.1 mm/rev	Workpiece microstructure, Chip morphology, Cutting force, Surface roughness, Cutting temperature, and Tool wear
[53]	Turning	Inconel 718	DED	Dry	V_c – 70–120 m/min a_p – 0.5 mm F – 0.1–0.2 mm/rev	Tool wear and Surface integrity
[54]	Turning	Inconel 718	SLM	Dry	V_c – 60 m/min a_p – 0.4 mm F – 0.12 mm/rev	Surface roughness and topography, Microhardness, Microstructure, and Tool wear
[55]	Turning	Inconel 718	SLM	Dry and Cold air	V_c – 60 m/min F – 0.08–0.2 mm/rev a_p – 0.4 mm	Surface roughness and topography, and Microhardness
[56]	Turning	Inconel 718	Laser cladding	Dry	V_c – 60–100 m/min a_p – 0.1–0.4 mm F – 0.1–0.3 mm/rev	Cutting force, Surface roughness, and Microhardness
	Milling				V_c – 10.24–12.69 m/min a_p – 0.1–0.5 mm F – 0.05–0.06 mm/tooth	
[58]	Milling	Inconel 625	LPBF	Dry	V_c – 30–90 m/min a_p – 0.1 mm F – 0.1–0.2 mm/tooth	Cutting force and Chip morphology
[59]	Milling	Inconel 939	DMLS	Dry	V_c – 30–50 m/min a_p – 0.25 mm F – 0.05–0.15 mm/tooth	Surface roughness and Hardness
[60]	Milling	Inconel 625	LPBF	Dry	N – 636.6–1910 rpm V_c – 30–90 m/min a_p – 0.1 mm F – 0.1–0.2 mm/rev	Cutting force, Tool wear, surface topography, and Chip morphology
[61]	Milling	Inconel 625	LPBF	Dry	N – 636.6–1910 rpm V_c – 30–90 m/min a_p – 0.1 mm F – 0.1 mm/tooth	Cutting force
[62]	Milling	Inconel 718	SLM	Dry, wet and MQL	V_c – 20–40 m/min a_p – 0.5 mm F – 0.05–0.15 m/min	Surface roughness
[63]	Milling	Inconel 625	SLM	Dry	V_c – 60 m/min a_p – 0.3 mm F – 0.05–0.15 mm/tooth	Surface topography, wear resistance, microhardness, and surface roughness
[64]	Milling	Inconel 718	LMD	Wet	N – 2500 rpm a_p – 0.75–1 mm F – 300 mm/min	Mechanical properties, Cutting force, Chip morphology, and Workpiece microstructure
[65]	Milling	Inconel 718	SLM	Dry	N – 25,000–30,000 rpm a_p – 0.05 mm F – 300 mm/min	Grain microstructure, Tool wear, Surface topography, Machined surface microhardness
[66]	Milling	Inconel 718	SLM	Dry	V_c – 55 m/min a_p – 0.3 mm F – 5–10 mm/min	Tool wear
[67]	Milling	Inconel 718	SLM	MQL	V_c – 90 m/min a_p – 0.1–0.2 mm F – 0.1 mm/tooth	Tool wear, and Surface integrity
[68]	Milling	Inconel 718	SLM	Dry and Wet	V_c – 30 m/min a_p – 0.5 mm F – 0.1 mm/tooth	Microstructure, Surface integrity, and Fatigue fracture of a workpiece
[69]	Drilling	Inconel 718	SLM	Dry	V_c – 15–30 m/min F – 0.025–0.075 mm/rev	Surface roughness and topography, Microstructure, and Microhardness

Table 1 – (continued)

Ref No.	Machining process	Workpiece material	AM process	Cooling/ Lubrication strategy	Machining parameters	Investigated machining responses
[70]	Wire EDM	Inconel 939	DMLS	Wet	Pulse on – 0.1–0.6 μs Pulse off – 3–12 μs Voltage – 80–200 V	Recast layer thickness and Surface roughness
[71]	Electrochemical	Inconel 718	LPBF	Electrolyte COOLPULSE ES-G8020	Potential difference – 7 V Current – 13 A Cycle time – 30 min	Downskin and Upskin surface integrity, and Working distance effect

Sartori et al. [73] examined the effect of workpiece material characteristics on machinability of the AMed Ti–6Al–4V produced by EBM and DMLS under the dry and cryogenic machining environments. Fig. 9 shows the microstructures of AMed and wrought titanium alloy. The finer acicular microstructure with 7% of fine lamellae α face and grain boundaries at β phase was observed with the EBMed sample (Fig. 9a). The DMLS sample exhibited a martensitic microstructure that contained only α' phase (Fig. 9b). The thermal conductivity investigation revealed that the EBM titanium alloy possessed higher thermal conductivity compared with the DMLS titanium alloy. The DMLS sample possessed lower thermal conductivity and higher hardness compared with EBM. The thermal and mechanical properties of the DMLS sample resulted in the deepest crater compared with the EBM sample when dry machining. However, the lower temperature generated during the cryogenic machining limited the diffusive wear which reduced the crater phenomenon when the machining of EBM sample.

Oyelola et al. [75] studied the surface integrity and the machining behavior when turning the AMed Ti–6Al–4V produced by DMD. Along the sample surface, the compressive stress was observed to be significant. The coated insert generated more compressive stresses in the parallel direction of the circumference compared with uncoated inserts. The porosity and the irregular deposition process generated from asymmetrical cooling had shown a remarkable impact on the machining behavior and the surface integrity of the final machined parts.

In another study, Oyelola et al. [81] investigated the machining behavior of Ti–6Al–4V/WC metal matrix composite (MMC) fabricated by DED during the turning process. The study reported that the MMC produced by AM possessed higher hardness compared with other production methods and thus it was very difficult to machine. The surface roughness of the single matrix part was in an acceptable range while the surface roughness of the MMC part was high. During the turning of MMC, the material pull-out phenomenon was prevalent which induced fatigue and crack initiation of the component. The MMC exhibited variation in hardness value which increased the cutting force and tool wear. However, the use of an adaptive machining system was proved beneficial to

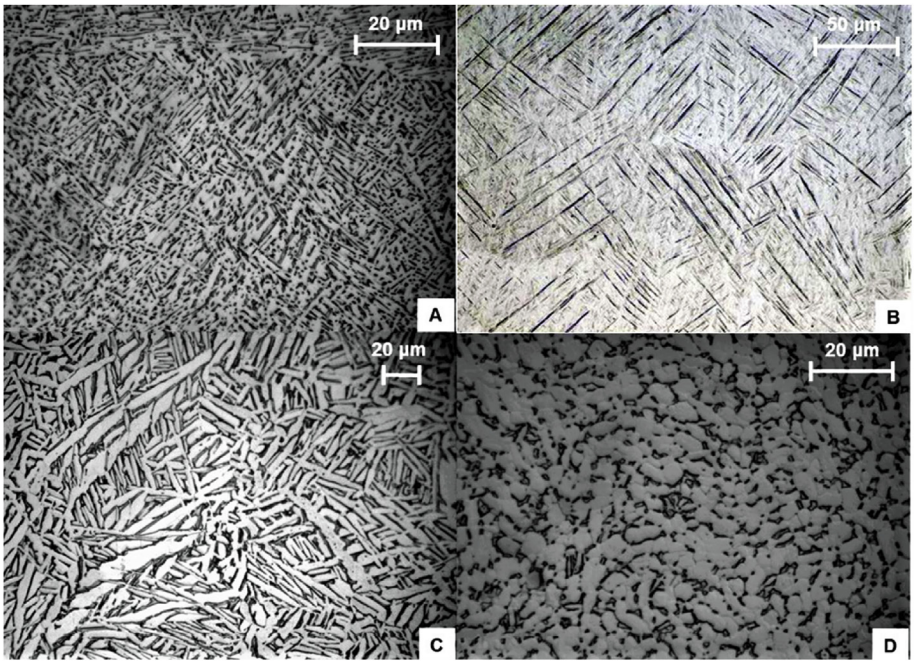

Fig. 9 – Microstructures of (a) EBM fabricated, (b) DMLS fabricated, (c) Heat-treated and (d) conventional Ti–6Al–4V [73].

enhance the surface roughness by controlling the machining parameters according to the variation in the microstructure. The interfacial layers of two materials possessed 40% higher hardness compared with other regions which caused significant tool wear.

Bruschi et al. [82] investigated the effect of cooling strategies and machining parameters on the tool wear during the turning of wrought and AMed Ti–6Al–4V fabricated by EBM. The cryogenic machining significantly reduced the friction and it assures the generation of adhesive wear instead of abrasive wear and hence the wear debris was being controlled which increased the tool life. The coefficient of friction was lower for both AMed and wrought Ti–6Al–4V using cryogenic machining compared with dry machining conditions.

Coz et al. [83] examined the machinability of the SLM-produced Ti–6Al–4V parts during the turning process. The generated cutting and feed forces were higher when machining of AMed titanium workpiece compared with cast titanium. The cutting forces were within 3–24% and 21–10% with increasing feed rate and cutting speed, respectively. The lower feed rate generated helical chips while the long chips were generated at higher feed rates. The cutting speed was observed to be more influential on the chip formation compared with the feed rate when the two-dimensional cutting of Ti–6Al–4V. The subsurface microstructure was not notably changed in micro-cutting compared with macro-cutting for both AMed and cast workpiece material.

Bordin et al. [86] studied the numerical analysis and machinability of the EBM produced Ti–6Al–4V when turning using cryogenic and dry cooling. The cutting force was predicted with a greater extent for all machining conditions using both dry and cryogenic cooling environments. Additionally, the proposed numerical model could precisely predict the movement of machining parameters to evaluate the machining behavior of the material in terms of severe deformed layer thickness and cutting temperature.

4.1.2. *Milling process*

The finish milling process is usually used by industries to achieve curved and flat surfaces. Huang et al. [87] compared the finish slot milling surface of AMed Ti–6Al–4V with wrought Ti–6Al–4V. The study revealed that the AMed workpiece had a better microstructure than that of a wrought workpiece. This better microstructure was responsible for the lower ductility and superior strength which ultimately resulted in a better finishing surface. An increase in machining feed increased the surface roughness. The AMed sample exhibited improved surface roughness compared with the wrought sample. The lower ductility of AMed titanium alloy is derived from the discontinued ridge topography during the milling process.

Veiga et al. [88] discussed the machinability and product quality when milling of AMed Ti–6Al–4V fabricated by PAW-WAAM. During the comparison among the down-milling and up-milling, the down-milling strategy seemed to be preferable in terms of torque generation. The tool path effect was the responsible factor for premature tool damage in the slot-milling process. The better surface quality was observed in the case of up-milling compared with down-milling. It was observed that the torque was more affected by the cutting speed than the depth in the perpendicular direction.

Bonaiti et al. [89] investigated the machining performance of AMed Ti–6Al–4V produced by LENS in terms of burr formation, cutting force, and surface quality during the micro-milling process. The increased laser power used during fabrication and finer martensite resulted in the high hardness of the AMed workpiece material. Additionally, a less porous surface was generated with an increase in the laser power which improved the overall surface integrity of the AMed material. The high hardness value caused this difficulty in machining and hence, reduced the surface roughness. However, the surface of conventionally produced Ti–6Al–4V was noticeably rougher than AMed Ti–6Al–4V. An increase in depth of cut and feed rate increased the surface roughness. The cutting force for the AMed sample was observed to be lower than that of the standard sample despite the higher hardness value of the AMed material. The significant burr formation was analyzed on the top of down milling for AMed sample while the very less amount of burr formation was examined after machining of standard material.

To overcome the manufacturing and machining problem associated with AMed material, Moritz et al. [90] designed a hybrid Ti–6Al–4V material which was produced by LMD and conventional machining methods. The additional layer was doped by LMD on the top of the conventional machined surface and the interface region was investigated for the induced defects. The cryogenic machining had provided better machining performance in terms of attained surface quality and tool life compared with the dry machining, observed through the lower surface defects, better surface roughness, and qualitative inspection of the tool damages. The formation of the organic residues on the machined surface could be avoided by cryogenic cooling compared with the dry machining, which was further proven by the fluorescence inspection. The analysis of the interface layer revealed that the conventional cooling residues generated surface porosity while the deposition of AMed surface after cryogenic machining was nearly defect-free. The vibration of the machine and workpiece at a higher cutting speed raised the surface roughness value.

The machining performance of conventional and EBM Ti–6Al–4V was compared by Hojati et al. [92] in micro-milling machining. The cutting force was notably affected by the chip thickness. The fine microstructure and high ductility provided higher strength to the EBM sample. Between the range of 7.4–37.3 μm of chip thickness, the cutting force was nearly the same due to the coarser microstructure but the cutting force was reduced by 5–15% when the chip thickness was less than 7.4 μm. In addition, the increasing cutting speed increased the strain rate at continuous chip thickness but did not affect the cutting force for extruded and EBM titanium workpieces. The greater uncut chip thickness dominated the thermal softening effect which increased the required cutting force for machining of both materials. At lower uncut chip thickness, the ploughing effect was increased, which substantially increased the specific cutting energy. Below 7.4 μm chip thickness, the specific cutting energy was raised by 5–15% for the extruded sample compared with the EBM sample due to the plastic deformation of the extruded sample shown in

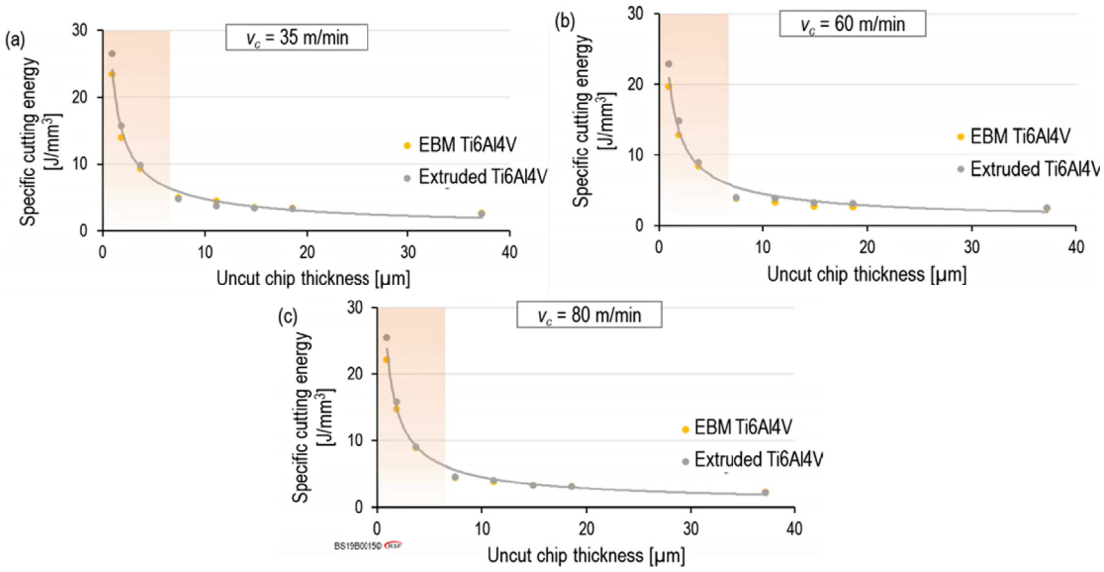

Fig. 10 – Impact of uncut chip thickness on the specific cutting energy at the cutting speed of (a) 35 m/min, (b) 60 m/min, and (c) 80 m/min [92].

Fig. 10. The higher hardness and high brittle feature of the EBM part cause lower plastic flow on the workpiece surface which produced a better-machined surface. A discontinuous burr was formed in the case of the EBM part while the continuous wavy burr was observed while the machining of extruded titanium.

Khaliq et al. [94] studied the surface quality, tool wear, and residual stresses when micro-milling of AMed Ti–6Al–4V produced by SLM, and also the lubri-cooling effect for the same was evaluated. Three major criteria of the tool rejection had been identified i.e. flank wear lower than 22 μm, cutting edge radius lower than 28 μm, and surface roughness lower than 0.5 μm. The limited width of the flank face made the flank wear as most critical factor of tool rejection. To lower the cutting force generated on the tooltip, the lower axial depth of cut was used which abruptly increased the cutting-edge radius, and consequently, the burr formation and surface roughness was increased. The flank wear was enhanced by 26.2% at 30 mm/min of constant feed rate and cutting speed while at fixed RPM of 35,000 and increasing feed rate, the flank wear was improved by 27.79% under MQL machining. The tool wear was improved by 26.21% at the 3500 RPM of cutting speed and the lowest feed of 30 mm/min with the MQL strategy. Additionally, the plowing effect was induced at the lower feed rate which caused the elastoplastic deformation, and hence, the residual stresses were increased. The higher cutting speed reduced the tool diameter and increased the cutting-edge radius and flank wear which was the most suitable condition for hard-to-cut material such as AMed titanium alloy. The better results for residual stresses and burr formation was observed with dry machining condition compared with MQL while MQL provided better results in terms of surface roughness, flank wear and reduced tool diameter.

Li et al. [95] analyzed the impact of temperature buildup on the cutting force during milling of AMed Ti–6Al–4V fabricated by DMD. The temperature buildup increased by 180 °C after deposition within the range of 20–120 s. During the simulation of the milling forces, the tool flank wear was not taken into consideration and hence, the forces measured by the simulation were lower than the measured forces. The milling force was notably decreased when the preheating temperature was above 300 °C. The milling force was decreased due to the thermal softening effect. The material flow stress was reduced because of an increment in cutting temperature with increasing preheating temperature. The work hardening effect was dominant over the thermal softening effect when the preheating temperature was below 300 °C. Furthermore, the increasing preheating temperature improved the thermal softening effect which ultimately decreased the milling force. The thermal softening effect was observed to be more obvious over the work hardening effect at low preheating temperature and higher feed/tooth. Over the 300 °C preheating temperature, the milling force increased which resulted in higher tool flank wear.

Campos et al. [96] compared the machinability of a commercial workpiece and AMed Ti–6Al–4V fabricated by SLM during the micro-milling process. The microstructure analysis revealed that the SLM-produced sample exhibited finer acicular α martensite structure with higher hardness and strength compared with the commercial sample. The SLM fabricated sample had shown more brittle behavior and lower stiffness than commercial material. Despite the 16% higher hardness value of SLM material than commercial material, the generated cutting force by SLM sample was 9.3% lower than commercial material. This can be attributed to the finer microstructure of SLM titanium material. The SLM-produced titanium yielded lower tool wear and the brittle characteristic of the SLM sample resulted in less plastic flow when machining which led to lower surface roughness during milling of the SLM workpiece compared with a commercial workpiece. The burr formation was higher in down milling compared with the up-milling process for both materials. The

smaller tool wear and less affected cutting-edge radius of the tool during the machining of the SLM workpiece resulted in lower burr formation compared with the conventional workpiece.

Oyelola et al. [99] carried out the milling and drilling of DED-produced Ti–6Al–4V by employing an adaptive control system. The remelted layer generated the anisotropy in the material during the deposition process which further influenced the material properties. This generated anisotropy had a major influence on the cutting force during the drilling process as it involved machining through the boundary layers. The adaptive control provided better surface roughness with fewer surface holes. The variation in the cutting force was prevented by applying the adaptive control system which was responsible for stable machining as shown in Fig. 11. By comparing both Fig. 11(a) and (b), it can be observed that the adaptive control system can adjust the system according to the variations in the microstructure at a higher feed rate which is beneficial to set the cutting force at a point. The adoption of the adaptive control system further eliminated the chatter marks when milling and provided enhanced surface roughness. Additionally, the deformation of the subsurface was reduced and the mechanical properties of the final produced part were better. Normally, the cutting force is increased with increasing feed rate which ultimately increases the deformations in the subsurface. However, the controller of the adaptive control system controlled the feed rate according to the cutting force, and hence the subsurface deformation could be reduced.

Hoye et al. [100] analyzed the machining performance in terms of generated cutting force of AMed Ti–6Al–4V fabricated by GTAW during the drilling and milling process. A thin wall structure of AMed Ti–6Al–4V was observed. The cutting force was reduced by 13–21% for AMed workpiece due to the lower hardness value of workpiece produced by GTAW compared with the wrought workpiece when milling. However, the fluctuating cutting force of the GTAW workpiece produced a 22.22% rougher machined surface compared with wrought material during the milling process due to the uneven thickness of the wall. In the case of drilling, the wrought billet exhibited 8% higher average hardness compared with AMed billet and thus the cutting force was increased by 15% when drilling of GTAW pad compared with the wrought pad. In addition, the tool wear on the tip of the chisel was higher for the wrought sample compared with the AMed sample. The GTAW produced workpiece exhibited better machining performance compared with a conventional workpiece.

4.1.3. *Drilling process*

Drilling is a very important finish machining process as it encapsulates almost all titanium applications. Rysava et al. [101] studied the micro-drilling of AMed Ti–6Al–4V produced by DMLS to identify the machinability. The exit burr of the hole was higher than the entrance burr which could create a fitting problem during the assembly of the parts. The measuring procedure to quantify the perpendicularity, diameter, and burr was proposed.

Alonso et al. [102] analyzed the effect of WAAM on machinability and mechanical properties during the drilling of titanium parts. The material properties revealed that the WAAM could be a feasible alternative to manufacture the titanium parts as it had not shown welding defects. The WAAM fabricated titanium parts needed higher cutting force and torque value because of high hardness. The cutting force increased with increasing feed/tooth, due to increased chip cross-sectional area. The serration mechanism in chip formation was observed during the metallographic inspection when drilling of WAAM fabricated part. The mechanical properties and the high hardness of the WAAM fabricated part was responsible for lower burr height compared with the conventional part. The WAAM fabrication process proved better in terms of burr height, mechanical properties, and machining performance except it required higher cutting force when drilling.

Dang et al. [103] analyzed the machining performance of AMed Ti–6Al–4V produced by DMLS when dry drilling. The

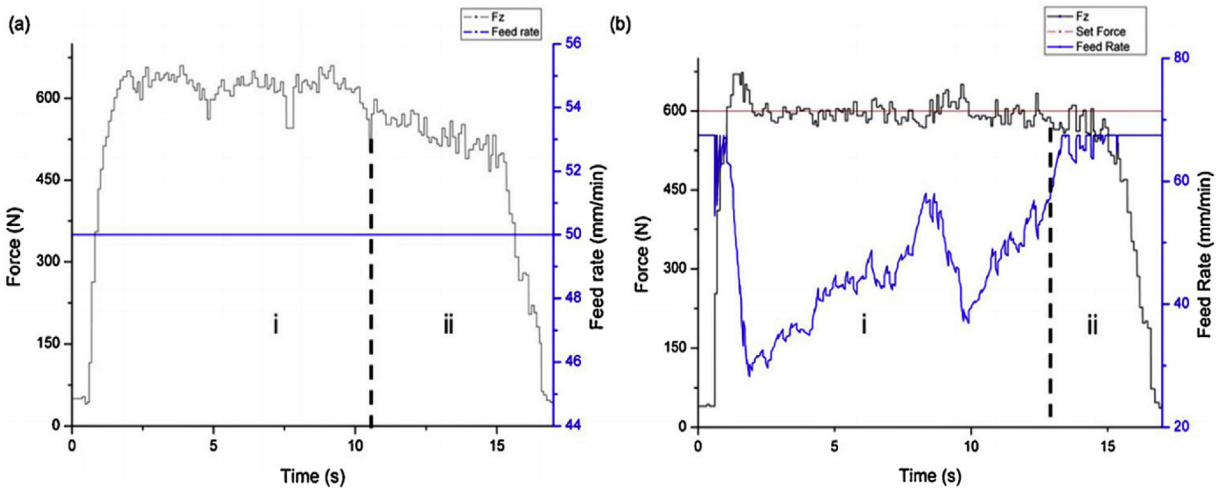

Fig. 11 – Cutting force variation after 16 passes (a) without implementing the adaptive control system at constant feed rate and (b) with implementing the adaptive control system with a constrained cutting force of 600 N during drilling of DED Ti–6Al–4V [99].

thrust force was deceased as the cutting speed was increased and the lowest thrust force was observed at 0.06 mm/rev of lower feed rate. The highest machining temperature was observed at 0.12 mm/rev feed rate and 1500 rev/mm cutting speed and hence it was concluded that the higher production can be achieved at a higher cutting speed and feed rate. The increasing feed rate lowered the surface roughness and minimum surface roughness was observed at 0.12 mm/rev feed rate and 800 rev/mm cutting speed. The prominent peeling-off phenomenon was noted on the rake face. Furthermore, abrasion and chip adhesion was detected on the rake face. The formation of the metamorphic layer occurred and it was increased with increasing tool wear and cutting temperature.

Ming et al. [104] studied the hole quality and the hip formation when drilling of DMLS fabricated Ti–6Al–4V under dry machining conditions. The varying cutting speed was led to the formation of different characteristics of chips such as the scaly, peak, and lamella on the different regions of the chip. The increasing feed rate was a responsible factor to reduce the shear angle and the generation of scratches and adhesion on the back surface of the chips. Thin strip-shaped and elongated grains were observed in the primary shear band while the secondary shear band was contained elongated β stage grains. The surface quality of the hole was remarkably affected by the chips. The severe scratches were observed on the hole surface due to chip clogging which was promoted by the alternation of the microstructure and defect-induced hole quality. The hole defects such as tearing, dragging, and cracks were mainly due to the particle plucking from the hole surface.

4.1.4. *Laser-assisted process (hybrid machining)*

Woo et al. [105] experimented with laser-assisted machining of DED-produced Ti–6Al–4V. The proposed two-path DED provided better shape accuracy and could eliminate the height and edge defect which was produced by using one path DED. The laser preheating had decreased the cutting force and surface roughness by 40% and 30% respectively. It was assumed that the hardness value of the workpiece was not changed even after machining because the hardness of material produced after the laser-assisted machining (400.52 HV) was in the acceptable range of hardness before the machining (396.28 HV). The chemical composition of the Ti–6Al–4V remained the same after laser-assisted machining using a preheated laser.

4.2. *Summary*

The literature survey for machining of AMed titanium alloys revealed that again AMed processes increase the hardness of titanium alloys which significantly increases the thrust force. The tool coating has a significant influence on the machining-induced residual stresses. The adoption of cryogenic cooling enhanced the tool life by lowering the coefficient of friction and the surface roughness was also improved. However, some controversial results were found in terms of the surface roughness of AMed titanium alloys. The MQL strategy was found to be better to enhance the residual stresses and burr formation when drilling the AMed titanium alloys. The synopsis of the literature review is presented in Table 2.

5. Tool wear

5.1. *Tool wear analysis of AMed nickel-based alloys*

Tool wear analysis is very essential for difficult-to-cut materials. Machining such metals/alloys lead to the reduction of the tool life due to various factors such as high affinity between tool-workpiece, high hardness at surprisingly high temperatures, poor thermal conductivity, and strain hardening which in turn dampers the processing ability of these materials [60]. Studies showed that tool wear in the machining of the wrought Inconel 718 is always greater than AMed Inconel 718. Furthermore, tool wear for AMed nickel-based superalloy Inconel 718 varies for distinct build orientations of the part, even though the hardness is identical. Park et al. [66] analyzed that the part treated with Hot Isostatic Pressing (HIP) has higher hardness when compared with as-built parts. But, the tool wearing is slower for HIP treated part while milling when compared with the part manufactured by vertical build orientation. The same authors found Abrasive wear to be a significant tool wear mechanism for both wrought and AMed alloys. They found Abrasive wear on the rake and flank faces of the tool; adhesive wear was also found on the rake face. Hard particles removing or displacing the tool material between the rake face of the tool and chip creates abrasive wear. On the other hand, Careri et al. [53] reported higher tool wear for heat-treated parts when compared with as-deposited parts. They reasoned the rapid tool wear for heat-treated parts as these parts have obtained better mechanical properties which lead to craters on the tool. The authors categorized tool wear mechanisms as abrasive, adhesive, and chipping, out of which abrasive is the significant mechanism influencing flank wear due to chips. Chipping was the result of the breaking of the cutting edges prompted by the adhesion of chips on the tools can be seen in Fig. 12. The direct contact of the workpiece and tool cutting edge resulted in adhesive wear which is shown by the purple zone in Fig. 12. This purple zone was subjected to a high force due to the beginning of chip formation which was the key point to start the tool wear. The green zone exhibits the delamination of tool coating due to the abrasion followed by adhesion mechanisms. The rubbing action between the tool surface and chip was the trigger point for damage caused on the tool coating. The increasing cutting parameters generated a partial chipping phenomenon that did not have any further effect on the produced surface quality. The induced plastic deformation triggered work hardening and due to this reason, the oriented and elongated grains were engendered along to the direction of cutting.

Chen et al. [52] reported a higher tool life of 2.64, 7.99, and 1.59 times for coated carbide tools compared with the cemented carbide tools for turning of the AMed Inconel 718 surface and subsurface and wrought Inconel 718, respectively. Cemented carbide tool predominantly posed nose wear and crater wear mechanisms for tool wear. The high-speed flowing of chips spawned crater wears on rake face; while, breaking of built-up edges (BUEs) involved TiC and NbC

Table 2 – Summary of literature review for conventional machining of AMed Titanium alloy.

Ref No.	Machining process	Workpiece material	AM process	Cooling/Lubrication strategy	Machining parameters	Investigated machining responses
[72]	Turning	Ti–6Al–4V	SLM	Dry	V_c – 45–180 m/min a_p – 0.5 mm F – 0.05–0.2 mm/rev	Cutting force and Surface roughness
[73]	Turning	Ti–6Al–4V	EBM and DMLS	Cryogenic (LN_2)	V_c – 80 m/min a_p – 0.25 mm F – 0.2 mm/rev	Tool wear
[74]	Turning	Ti–6Al–4V	EBM and DMLS	Dry and Cryogenic (LN_2)	V_c – 80 m/min a_p – 0.25 mm F – 0.2 mm/rev	Tool wear
[75]	Turning	Ti–6Al–4V	DMD	Dry	V_c – 70 m/min a_p – 1.25 mm F – 0.15 mm/rev	Surface integrity
[76]	Turning	Ti–6Al–4V	DMLS	Cryogenic (LN_2) and Dry	V_c – 80 m/min a_p – 0.25 mm F – 0.1–0.2 mm/rev	Surface integrity
[77]	Turning	Ti–6Al–4V	EBM	Cryogenic and Dry (LCO_2)	V_c – 50–80 m/min a_p – 0.25 mm F – 0.1–0.2 mm/rev	Chip morphology, Tool wear, and surface integrity
[78]	Turning	Ti–6Al–4V	EBM	Cryogenic (LN_2) and Dry	V_c – 50–80 m/min a_p – 0.25 mm F – 0.1–0.2 mm/rev	Tool wear
[79]	Turning	Ti–6Al–4V	EBM	Wet	V_c – 50–80 m/min a_p – 0.25 mm F – 0.1–0.2 mm/rev	Tool wear, chip morphology, microstructure, and surface integrity
[80]	Turning	Ti–6Al–4V	EBM	Dry, Flood and Cryogenic (LN_2)	V_c – 80 m/min a_p – 0.25 mm F – 0.1–0.2 mm/rev	Microstructure, Mechanical properties, Surface defects and topography and corrosion behavior of the workpiece
[81]	Turning	Ti–6Al–4V	DED	Wet	V_c – 80 m/min a_p – 0.025–0.05 mm F – 0.1 mm/rev	Microstructure, Surface roughness, Cutting force, and tool wear
[82]	Turning	Ti–6Al–4V	EBM	Cryogenic (LN_2) and Dry	V_c – 50–80 m/min a_p – 0.25 mm F – 0.1–0.2 mm/rev	Surface characteristics, Friction analysis, and Sliding wear
[83]	Turning	Ti–6Al–4V	SLM	Dry	V_c – 6–500 m/min F – 0.001–0.02 mm/rev	Cutting force, Chip morphology, and Microstructure,
[84]	Turning	Ti–6Al–4V	EBM	Cryogenic (LN_2) and Dry	V_c – 80 m/min a_p – 0.25 mm F – 0.1 mm/rev	Microstructure, and Surface defects and topography
[85]	Turning	Ti–6Al–4V	LPBF	Cryogenic (LN_2) and Dry	V_c – 80 m/min a_p – 0.5 mm F – 0.2 mm/rev	Microstructure and Surface integrity
[86]	Turning	Ti–6Al–4V	EBM	Cryogenic (LN_2) and Dry	V_c – 50–110 m/min a_p – 0.2 mm F – 0.1–0.2 mm/rev	Cutting force and Cutting temperature
[87]	Milling	Ti–6Al–4V	LAM	Dry	N – 200 rpm a_p – 0.5 mm F – 0.01–0.13 mm/tooth	Microstructure and Surface topography
[88]	Milling	Ti–6Al–4V	WAAM (PAW)	Dry	V_c – 50–60 m/min a_p – 0.4 mm F – 0.066–0.12 mm/tooth	Microstructure, Mechanical properties, Torque, Surface quality, and Tool breakage

Table 2 – (*continued*)

Ref No.	Machining process	Workpiece material	AM process	Cooling/Lubrication strategy	Machining parameters	Investigated machining responses
[89]	Milling	Ti–6Al–4V	LENS	Wet	N – 16,000 rpm V_c – 25.5 m/min a_p – 0.025–0.075 mm F – 0.02–0.03 mm/tooth	Surface roughness, Cutting force, and Burr formation
[90]	Milling	Ti–6Al–4V	LMD	Cryogenic and Dry (LCO_2)	V_c – 100–115 m/min a_p – 0.1 mm F – 0.075–0.1 mm/tooth	Chip morphology, Tool wear, Surface roughness, and Microstructure
[91]	Milling	Ti–6Al–4V	LPBF	MQL	N – 11,937 rev/min V_c – 75 m/min a_p – 0.2 mm F – 0.02 mm/tooth	Chip morphology, Tool wear, and surface roughness
[92]	Milling	Ti–6Al–4V	EBM	Wet	V_c – 35–80 m/min a_p – 0.3 mm F – 0.00125–0.05 mm/tooth	Surface quality, Cutting force, Specific cutting energy, and Burr formation
[93]	Milling	Ti–6Al–4V	LPBF	MQL	V_c – 30–60 m/min a_p – 0.2 mm F – 0.01–0.05 mm/tooth	Mechanical properties, Surface topography and surface texture, Surface defects, Burr extent, and chip morphology
[94]	Milling	Ti–6Al–4V	SLM	Dry and MQL	N – 15,000–35,000 rpm V_c – 23.6–55 m/min a_p – 0.075 mm F – 30–90 mm/min	Surface quality, Tool wear, and Residual stresses
[95]	Milling	Ti–6Al–4V	DMD	Dry and water cooling	N – 4000 rpm a_p – 0.6 mm F – 0.05–0.13 mm/tooth	Cutting force, Tool flank wear, and Subsurface deformation
[96]	Milling	Ti–6Al–4V	SLM	Dry	N – 18,000 rpm V_c – 28.3 m/min a_p – 0.04 mm F – 0.005–0.04 mm/tooth	Cutting force, Chip morphology, Burr height, and Surface roughness
[97]	Milling	Ti–6Al–4V	DMLS	Dry	V_c – 150–250 m/min a_p – 0.5 mm F – 0.05–0.09 mm/tooth	Cutting force, Chip morphology, Surface quality, and Tool wear
[98]	Milling	Ti–6Al–4V	EBM	–	V_c – 24.384–48.768 m/min a_p – 0.635–905 mm F – 0.0127–0.0381 mm/tooth	Microstructure, Cutting force, and Surface integrity
[99]	Milling	Ti–6Al–4V	DED	Wet	N – 780 rpm a_p – 0.5 mm F – 0.035 mm/tooth	Subsurface deformation,
	Drilling				N – 500 rpm F – 50 mm/min	Surface roughness and Cutting force
[100]	Milling	Ti–6Al–4V	GTAW	Wet	V_c – 80 m/min a_p – 1 mm F – 0.15 mm/tooth	Cutting force, Microhardness, and Surface roughness
	Drilling				N – 571 rev/min V_c – 9 m/min F – 0.09 mm/rev	
[101]	Drilling	Ti–6Al–4V	DMLS	Dry	V_c – 60–110 m/min F – 0.01–0.02 mm/tooth	Hole quality
[102]	Drilling	Ti–6Al–4V	WAAM	MQL	V_c – 10–30 m/min F – 0.05–0.1 mm/tooth	Microstructure, Mechanical properties, Chip morphology, Cutting force, and hole quality

(*continued on next page*)

Table 2 – (*continued*)

Ref No.	Machining process	Workpiece material	AM process	Cooling/Lubrication strategy	Machining parameters	Investigated machining responses
[103]	Drilling	Ti–6Al–4V	DMLS	Dry	N – 500–1500 rev/min F – 0.06–0.15 mm/rev	Tool wear, Cutting temperature, Chip morphology, Surface roughness, and Cutting force
[104]	Drilling	Ti–6Al–4V	DMLS	Dry	N – 500–1500 rev/min F – 0.06–0.15 mm/rev	Hole quality and Chip morphology

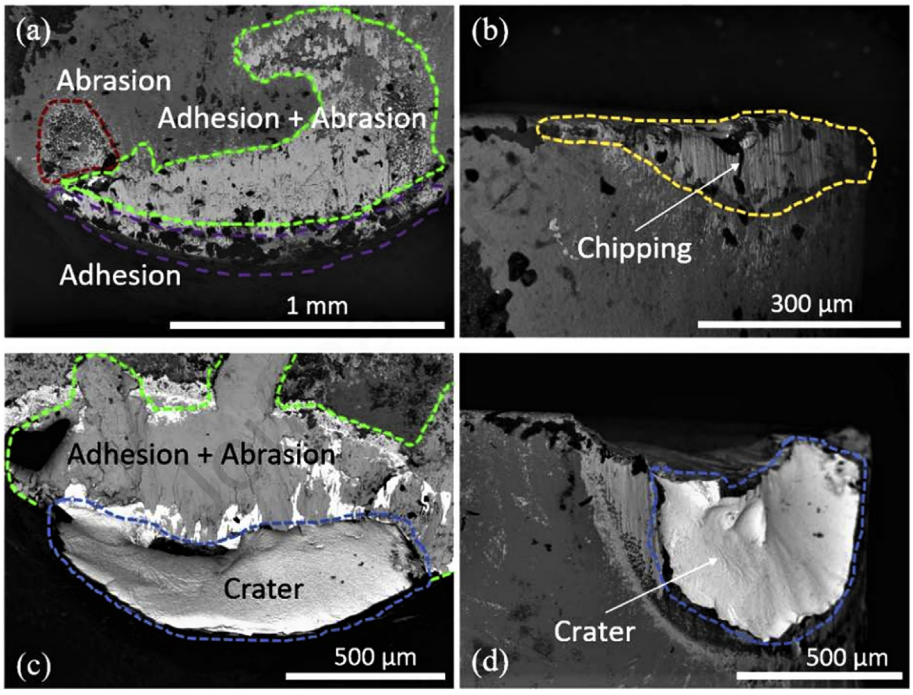

Fig. 12 – The dominant wear mechanism of tool tip during turning of Inconel 718 at $V_c = 120$ m/min, $F = 0.2$ mm/rev and $a_p = 0.5$ mm (a) and (b) for as-deposited sample, (c) and (d) for heat-treated sample [53].

particles in the cutting process inducing nose wear. Significant tool wear mechanisms for coated carbide tools were crater wear, nose breaking, and coating peeling. The high surface roughness of the parts catered into faster tool wear due to the nose wear and craters wear. While machining the Inconel 718 part subsurface using a coated carbide tool resulted in the longest tool life crater wear in the tool wear mechanism, coating peeling, and notch wear. Fei et al. [60] found that the fracture edge chipping is the predominant tool wear mechanism for the finish milling of Inconel 625 parts. Other mechanisms include coating peeling and delamination, notch wear, crater wear, flank wear, and BUEs.

5.2. *Tool wear analysis of AMed titanium-based alloys*

Sartori et al. [73] conducted turning experiments on the Ti–6Al–4V parts that were produced using EBM, DMLS, heat-treated DMLS part and wrought part under dry and cryogenic conditions. The authors found that chips have adhered and welded to the tool rake face and the cutting edge regardless of the cutting condition. Cryogenic turning substantially reduced the depth of the crater for all the workpieces when compared with the dry environment. Dry turning of DMLS workpiece resulted in deepest crater measuring 52.3 µm; the reason being in this work two mechanical properties namely thermal conductivity and hardness are considered to be a predominant factor for crater wear. Thus DMLS workpiece had the lowest thermal conductivity and highest hardness amongst all the workpieces studied in this study, also the heat generated in the cutting zone plays a major role. The rapid heat losses by using cryogenic LN_2 in the cutting zone reduces the size of craters formed and as mentioned earlier, adhesive and diffusive wear are reserved. The generation of crater wears mainly occurred due to some material properties such as thermal conductivity and hardness. The higher hardness and lower thermal conductivity were the main affected properties of the DMLS titanium alloy which prevented the complete elimination of the crater

phenomenon during the turning of alloys printed by DMLS. The deviation in mechanical and thermal properties brought the deepest depth of crater wear in the dry machining condition. In another study, Sartori et al. [74] analyzed the tool wear mechanism under the dry and cryogenic cooling conditions for turning AMed Ti–6Al–4V parts that were produced by DMLS and EBM technologies. The higher hardness and lower thermal conductivity resulted in the deepest crater depth on a tool with DMLS titanium alloy using a dry machining environment. The usage of cryogenic cooling reduced the cutting temperature significantly. This resists the diffusive wear and consequently, the crater formation could be avoided. The cryogenic cooling had efficaciously eliminated the crater wear when turning of EBM titanium alloys while the reduction of 58% in crater formation was detected during machining of DMLS titanium alloy compared with the dry machining as shown in Fig. 13. The reduction of the flank wear and cutting-edge abrasive wear was analyzed using a cryogenic cooling strategy with a heat-treated DMLS workpiece sample. The tool wear was analyzed based on thermal and mechanical properties of the workpiece, which were temperature-dependent. The best machinability was provided by the EBM workpiece sample as it showed a better thermal conductivity and lower hardness compared with the DMLS sample.

Bordin et al. [77] used coated carbide tool for turning EBM Ti–6Al–4V under dry, wet, and cryogenic LN_2 cutting conditions. The tool wear was always less for every combination of cutting parameters for cryogenic turning compared with the other two. Cryogenic coolant also prevented nose wear and cratering in the tool while turning effectively reducing tool wastage. The common reason for crater wear is an accumulation of excessive heat at the cutting zone, due to which cryogenic coolant can effectively prevent it while dry and wet coolant cannot. Higher temperature also aids adhesion of workpiece material on the tool surface, as a result during dry and wet turning authors found more adhered materials on the tool as compare to cryogenic turning. The authors found that the adhesion wear was a significant wear mechanism that successfully endorses the sticky nature of EBM Ti–6Al–4V. Fig. 14 shows adhesion in pastel gray color for this study, adhesion aids BUEs and craters in the tool during dry and wet turning. In another recent study by Bordin et al. [78] analyzed the tool wear mechanism on coated carbide tool during semi-finish turning of AMed Ti–6Al–4V fabricated by EBM with dry and cryogenic machining conditions. The adhesive tool wear was the dominant wear mechanism for both dry and cryogenic machining conditions. The formation of crater wear could be prevented by cryogenic cooling by lowering the machining temperature tool/workpiece interface even for critical machining parameters. The reduced length of chip-tool contact proved that the cooling capacity of cryogenic strategy had prevented the workpiece material adhesion on rake face and cutting edge.

As machining time increased, the adhered layer thickness on the rake face was reduced under cryogenic cooling compared with dry machining. In the dry machining condition, the erosion and abrasion caused the cutting-edge chipping; however, the cutting edge was finely protected by adhered workpiece material with cryogenic turning. Fig. 15 exhibited the dominant wear mechanism under the dry and cryogenic machining conditions.

In another study, Bordin et al. [79] performed experiments on turning of EBM and wrought rods made of Ti6Al4V under dry and wet using emulsion conditions using coated WC tool. In this study, adhesive wear was reported as a major wear mechanism for both the workpieces and bot the cutting conditions used, while, crater wear mechanism was only found in EDM Ti alloy. The reasons for these wear mechanisms were the same as discussed in the analysis above. Moritz et al. [90] studied milling of LMD Ti6Al4V by ball nose cutter coated by TiAlN under a cryogenic and dry cutting environment. The used tool for cryogenic milling displayed minuscule wear even though it completed a pre-defined milling length of 90 m, whereas, during dry machining, the tool failed after hardly 60 m of the milling length. Flaking of tool edge was clearly visible during dry machining but hardly apparent for cryogenic machining. Also, Ti materials were adhered to the tool under dry conditions, whereas no Ti BUEs were found for cryogenic milling. The authors concluded that the tool life can be increased by a factor of 1.5 using cryogenic conditions for machining the LMD manufactured parts, which are made of Ti6Al4V.

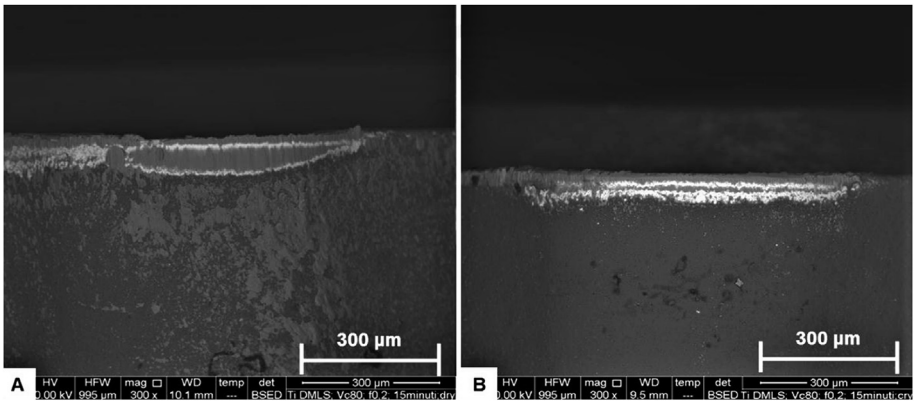

Fig. 13 – Tool flank image after 15 min when the turning of DMLS Ti–6Al–4V under (a) dry machining condition and (b) cryogenic cooling (LN_2) [74].

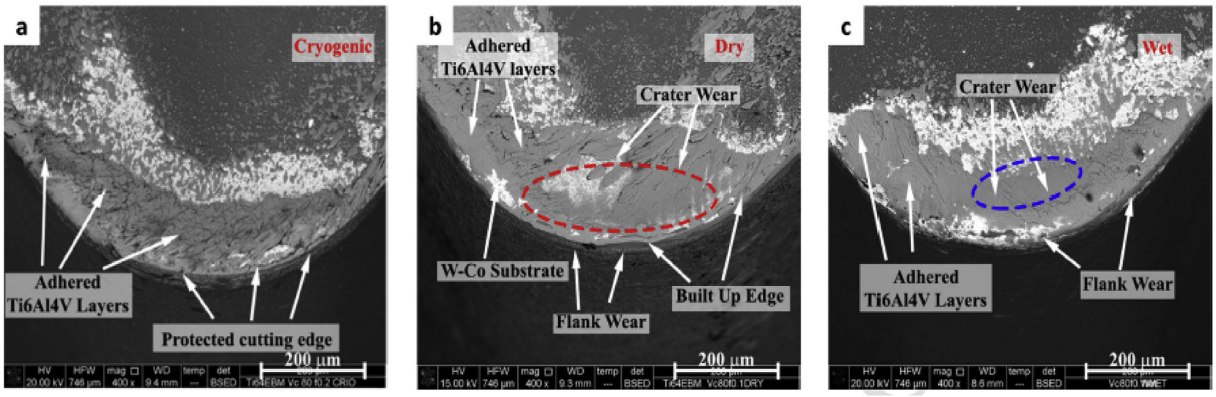

Fig. 14 – Images of tool worn faces after 15 min when turning EBM Ti–6Al–4V at 80 m/min of cutting speed and 0.2 mm/min of feed rate under a) cryogenic cooling, b) dry machining, and c) wet machining [77].

Lizzul et al. [91] studied the effect of anisotropy on the tool wear for milling of AMed Ti–6Al–4V parts fabricated by LPBF technology. The part had been manufactured in four different build-up orientations to analyze the effect of machinability on diverse orientations. It was observed that the favorable grain growth was lateral to the build direction without any impact of the inclination angle, which was responsible for the formation of microstructural anisotropy. The cutting tool wear was significantly affected by the different orientations of the build-up. The 40% of reduction in tool life was observed by increasing the orientation angle from 0° to 90°. The radius of the worn cutting edge was also increased during the milling operation at 90° angle, which generated the ploughing phenomenon, and hence the smoother surface was produced. As the tool wear increased, the burr formation and surface defects were increased. Furthermore, the amount of the adhered material on the machined surface was also increased by increasing tool wear. The shearing mechanism occurred when the cutting was brought lamellar ribbon-like chips. Further, Zhang et al. [97] employed ceramic tools while high-speed milling of DMLS Ti6Al4V part. Due to the high-speed machining, higher temperatures will be generated along with friction between chips, enormous sliding velocity, and high friction stress which forces tool rake face for faster wear and tear. The tool undergoes a high temperature of almost 1000 °C and cutting forces in the range of 400–500 N. It can be deduced from Fig. 16 that; abrasive and adhesive wear mechanisms are induced on the tool. The flank face of the tool significantly poses with abrasive and adhesive wear; while the rake face predominantly poses an adhesive wear mechanism. Different wear occurred on the rake and flank faces that are adjacent to the cutting tool. This specifies that the diffusion takes place under recurring mechanical and thermal loads. The authors ascribed the tool wear occurrence to robust extrusion among other tools under extreme cutting conditions and the specimen, and the high friction produced due to hard particles of the specimen.

After analyzing the tool wear section, it can be found out that abrasive wear is the main wear mechanism for Inconel 718. Further, even though the hardness of Inconel 718 built by different orientations is similar, the tool wear rate can be different. This assertion is proved when Park et al. [66] reported a higher wear rate for a vertically oriented AMed part compared with the heat-treated part, even though the hardness is higher for the latter. One of the other studies contradicted the result of previous authors, they found the tool wear rate for a heat-treated part to be lower than for a part AMed. It can be also analyzed that coated carbide tools are better than cemented carbide tools specifically for Inconel 718 in terms of enhanced tool life while nose and crater wear has been identified as a significant wear mechanism for cemented carbide. Machining Inconel 625 poses fracture edge chipping wear mechanism as primary compared with others. For Ti alloys, it has been found that adhesion wear is the significant wear mechanism followed by crater wear. The cryogenic cutting condition results in lower tool wear when the adhesion of workpiece material on the tool and cratering is reduced due to the reduced heat generated at the tool–workpiece interface, and this reduces the diffusion of the coating. Thus, a cryogenic environment is recommended for machining AMed titanium and nickel-based alloys which can increase tool life by the factor of 1.5. DMLS Ti alloys were found to be the hardest material, the lowest thermal conductivity with the largest tool wear rate among other materials. On the contrary, the highest machinability was observed in the EBM Ti alloy.

6. Surface integrity

6.1. *Surface integrity analysis of AMed nickel-based alloys*

The surface integrity of any component needs special attention, which should mitigate the required final product of the industry. The surface integrity of the machined product is dependent on the tool wear, machining parameters, and cooling condition. Careri et al. [53] observed that the limited tool wear occurred and a considerable reduced the surface roughness at the lower feed rate during the turning of Inconel 718. In addition, the reduced cutting speed also decreased the surface roughness according to the material condition. The heat-treated Inconel 718 possessed the worst surface integrity at a higher feed rate due to the higher tool wear. Furthermore,

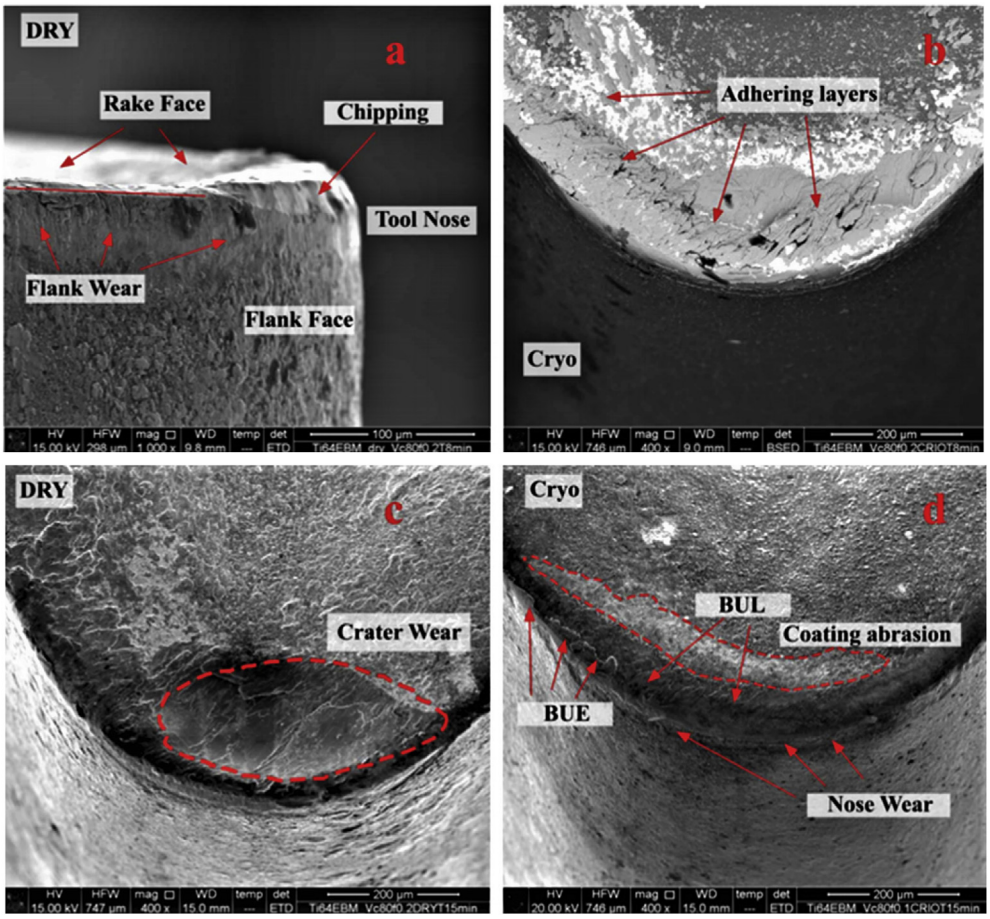

Fig. 15 – The dominant tool wear mechanism induced after 8 min of turning of EBM Ti–6Al–4V at $V_c = 80$ m/min and $f = 0.2$ mm/rev under (a) and (c) dry, and (b) and (d) cryogenic machining conditions [78].

the increment in cutting speed also led to the failure behavior of the tool in terms of low surface roughness; hence, it was revealed that the higher cutting speed was not preferable to machine the heat-treated Inconel 718 with better surface integrity. Post-process machining such as vibratory surface finish (VSF), finish machining (FM), drag finish (DF), and finish machining (FM) enhanced the surface roughness of the AMed nickel-based components. The DF process provided promising results in terms of lower surface roughness and better surface integrity in terms of surface and subsurface microstructure and microhardness compared with the VSF process and VSF was not enable to remove the surface powder from the AMed part after the SLM process. The arithmetic average surface roughness of the SLMed component was reduced by 96% and 88% using the FM and DF finishing process compared with an as-built component of Inconel 718. The finish machining process increased the surface hardness by 21% while the drag finish and vibratory surface finish exhibited a 10% of increment in surface hardness of the SLM component compared with the as-built component. Additionally, the study divulged that the wear performance of the SLM fabricated Inconel 718 could be improved by the post processes. The finish machining and drag finish processes reduced the wear rate of the SLM component by 12% and 7% respectively [54]. Kaynak and Tascioglu [55] investigated the machining-induced microhardness and surface roughness during the semi-finish turning of AMed Inconel 718 produced by SLM. The study revealed that the surface roughness of as-built AMed components could be significantly reduced by the finish machining processes. The resulted work hardening was affected by the finish machining, which increased the microhardness of the SLMed Inconel 718 component. The microhardness was boosted with increasing feed rate, and as a result, a high microhardness was observed at 0.2 mm/rev out of 0.08–0.2 mm/rev range of feed rate. Furthermore, the effect of the feed rate on microhardness and surface roughness of the SLMed Inconel 718 was exposed. Fig. 17 exhibited the surface roughness of the SLMed Inconel 718 alloys as a function of feed rate and cooling conditions. The 92% of the decrement in surface roughness was noted for SLMed Inconel 718 after the finish machining process compared with as-built SLMed Inconel 718 and with decreasing feed rate the % of decrement in surface roughness was increased as exhibited in Fig. 17.

During the face milling of AMed Inconel 625 fabricated by LPBF [60], the authors observed the jagged feed marks for all machining conditions. The gasification occurred during the LPBF process which induced the pores on the surface of the AMed Inconel 625 component which resulted in poor surface integrity. The finish milling process was proved worthier to

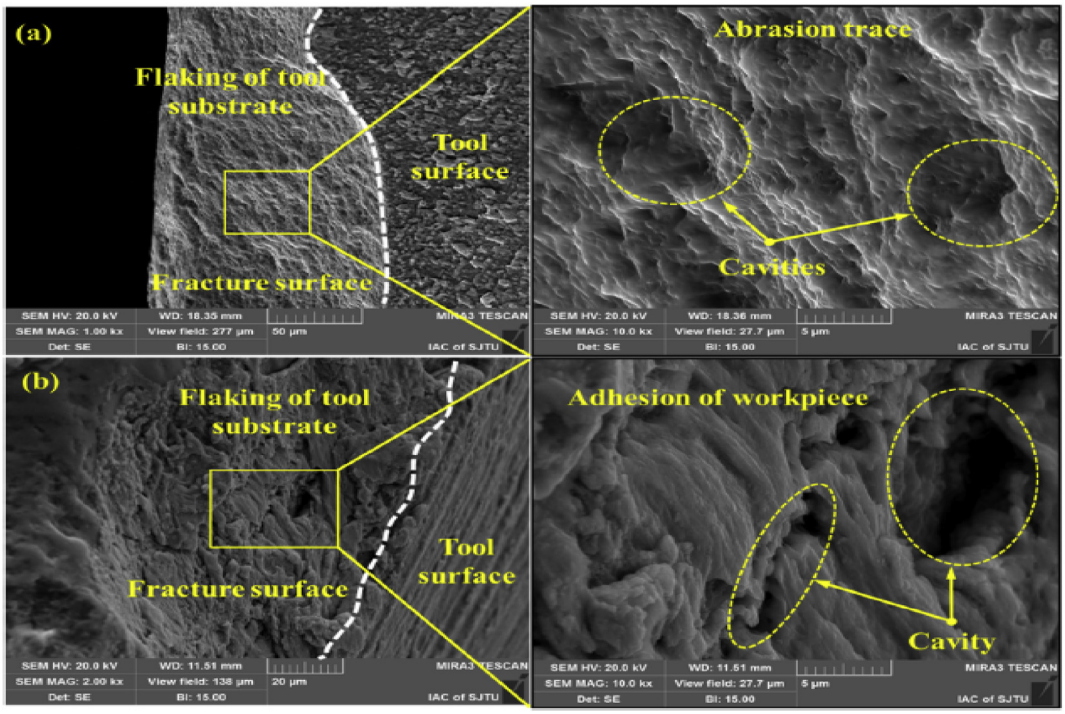

Fig. 16 – An illustration showing the types of wear such as (a) abrasion marks and, (b) workpiece adhesion [97].

reduce the AM process-induced pores up to a better extent. The left welded particles during machining resulted in the smeared and adhered material on the machined surface which deteriorated the final product surface integrity. The tool vibration at a higher temperature when milling triggered the plastic deformation of the surface material which led to the material side flow along with jagged feed marks. Tascioglu et al. [63] analyzed the surface integrity of AMed Inconel 718 after the post-milling process. The study divulged that the surface along the building direction was highly rough compared with the surface along the scanning direction. The surface of the SLMed component was become discontinuous due to the attachment of partially melted powder on the outer surface of the sample. The post-processed surface topography of the AMed Inconel 718 was much consistent and smoother. The measured surface roughness on the building direction was 50% higher than that of the scanning direction for the as-build specimen. Sadiq et al. [67] studied the effect of milling parameters, scanning strategy of SLM, and tool coating on the surface roughness during the micro-milling of SLMed Inconel 718. The SLM process-induced slags and inclusion, partially welded powder sphere, cavity shrinkage, and microcracks as shown in Fig. 18. It was observed that the uncoated WC tools were not useful since they provided higher surface roughness and lower tool life. However, AlTiN/Si_3N_4 coated cutting tool has provided better surface roughness compared with AlTiN coated tool during machining. The higher hardness of the SLMed Inconel 718 caused more difficulty to machine the component compared with extruded Inconel 718 component. The finishing micro-milling process reduced the surface roughness by 88%; however, the machined surface contained slags and pores which weakened the effectiveness of the finish machining process.

Periane et al. [68] studied the surface microstructure of SLMed Inconel 718 after milling under dry and emulsion cooling. The deformed and coarsened grain microstructure was observed on the dry machined surface. The pressurized thermomechanical load acting on the machining surface resulted in deformed and coarsened grains. This deformed grain region within the range of 50 μm from the machined surface was unveiled higher resistance to the fatigue crack instigation and propagation and hence the dry machining component resist the more fatigue cycle compared with the emulsion machining. The emulsion environment reduced the thermal effect during the machining and hence it persuaded a few deformed layers on the machined surface which caused less fatigue resistance and during the application of fatigue load, the crack initiation and propagation began from the edge of the sample. The aeronautic heat treatment and hot isostatic pressing significantly reduced the surface porosity and enhanced the hardness by 35% compared with an as-built component. The emulsion condition unveiled lower cutting force and higher surface roughness compared with the dry machining. The thermal subsurface was removed in the emulsion environment which caused the crack initiation and propagation. Karabulut and Kaynak [69] have conducted the drilling experiment on the AMed Inconel 718 fabricated by SLM to exemplify the impact of the machining parameters on the hole surface integrity. The smoother surface was obtained with a lower feed rate of 0.025 mm/rev and a higher cutting

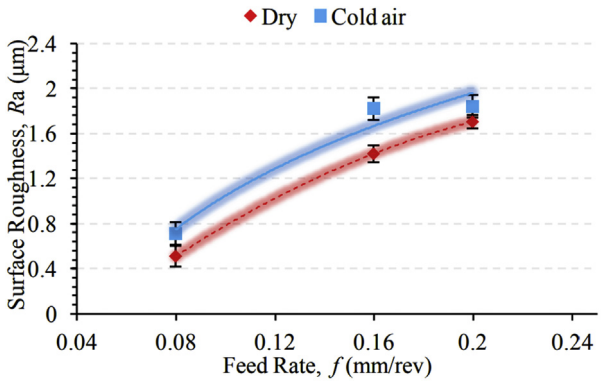

Fig. 17 – Surface roughness as a function of variation in the feed rate of AMed Inconel 718 [55].

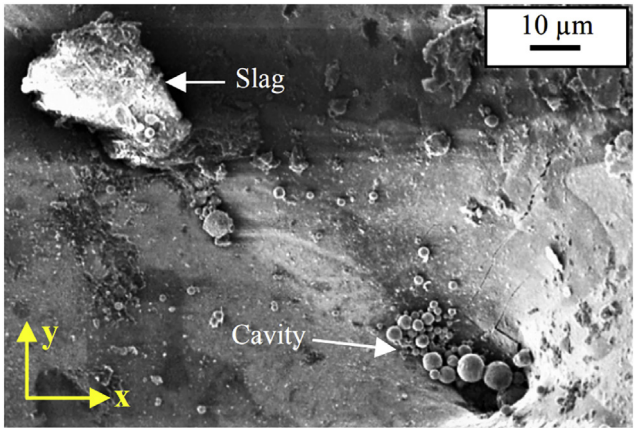

Fig. 18 – AMed induced surface defect on the Inconel 718 after SLM [67].

speed of 30 mm/min. At all feed rates, the feed mark on the machined surface was observed. The drill bit was facing difficulties to machine the hard surface at a high cutting speed and feed rate. The scratches and debris were observed on the surface at a high feed rate and cutting speed as shown in Fig. 19. The plastically deformed layers were formatted on the hole surface and the boundaries of the melting pool were nearly vanished due to the generation of high temperature during machining. The microhardness of the hole surface was increased due to the increase in the feed rate and cutting speed.

6.2. *Surface integrity analysis of AMed titanium-based alloys*

Sartori et al. [76] investigated the surface integrity of AMed Ti–6Al–4V fabricated by DMLS during turning with a cryogenic cooling strategy. An irregular and jagged induced surface was observed using LN_2 compared with dry machining conditions as shown in Fig. 20. The smeared and adhered material of dry machining (Fig. 21) was successfully eliminated by the cryogenic cooling, though the use of cryogenic cooling caused irregular surfaces with feed marks. The size of the tearing phenomenon was reduced by cryogenic cooling. The surface compressive stress was increased by 50% and 30% with cryogenic cooling compared with dry cooling when turning was performed on the DMLS and heat-treated DMLS samples, respectively. Both the layer of compressive residual stress and axial residual stresses were induced by employing the LN_2.

Bordin et al. [77] compared the surface integrity of AMed Ti–6Al–4V under dry, wet, and cryogenic cooling. It was observed that the surface roughness was significantly impacted by the feed rate compared with the cutting speed. The use of LN_2 decreased the crater and flank wear, which ultimately resulted in a reduction of surface roughness. The tool flank wear was highly affected by surface roughness. There was no direct contact between the tool flank and the workpiece, which resulted in limited abrasive wear. This reduced the effect of the cooling strategies while the AM parts were being subjected to finish machining. The wet turning of the AMed titanium showed double-feed marks, adhered particles, long grooves, and side flow of material on the surface of the machined part as shown in Fig. 22. The ploughing action of the cutting edge incurred the long grooves between two following feed marks. Due to the rubbing action between the tool and the workpiece, the BUE detached in small fragments, and when these fragments passed under the rake face of the tool, it deserted the grooves on the machined surface. The material that was left during the turning was welded to the surface, which resulted in adhered material on the finished turned part.

Bordin et al. [79] compared the machining behavior of AMed and wrought Ti–6Al–4V. The authors found that the profile shape of the surface was not affected by tool wear at all the cutting parameters. However, the surface topography was impacted when the tool wear exceeded the value of 0.1 mm. The adhered material formed a protective layer on the surface and the wet machining caused a reduced rubbing action, resulting in the cutting speed has a negligible effect on the surface topography. The lower ductility of the EBM Ti–6Al–4V affected the mechanism of chip formation, which resulted in a higher surface roughness value for the EBM sample. An analysis of the microstructure of the machined wrought and EBM samples exhibited a thin deformed layer of the material on the surface cross-section that was parallel to the cutting direction. However, the depth of this deformed layer was very similar for both alloys. The work hardening effect occurred due to the surface hardening during the turning process. The values of microhardness increased at the higher cutting parameters. This could be attributed to the generation of a high mechanical and thermal load on the workpiece at the higher cutting parameters. Bertolini et al. [80] studied the surface integrity of machined Ti–6Al–4V produced by EBM AM under cryogenic, flood, and dry machining conditions. The EBM sample was found to be more sensitive towards the induced hardening effect from machining and the generation of compressive stresses. Cryogenic cooling caused more hardening and a thicker deformed layer on the machined surface. The surface of the EBM workpiece was rougher, compared with the results of conventional processes, and this was due to the greater hardness of the EBM workpiece. Traces of smeared feed marks and adhered material were insignificant under cryogenic cooling compared with dry and conventional

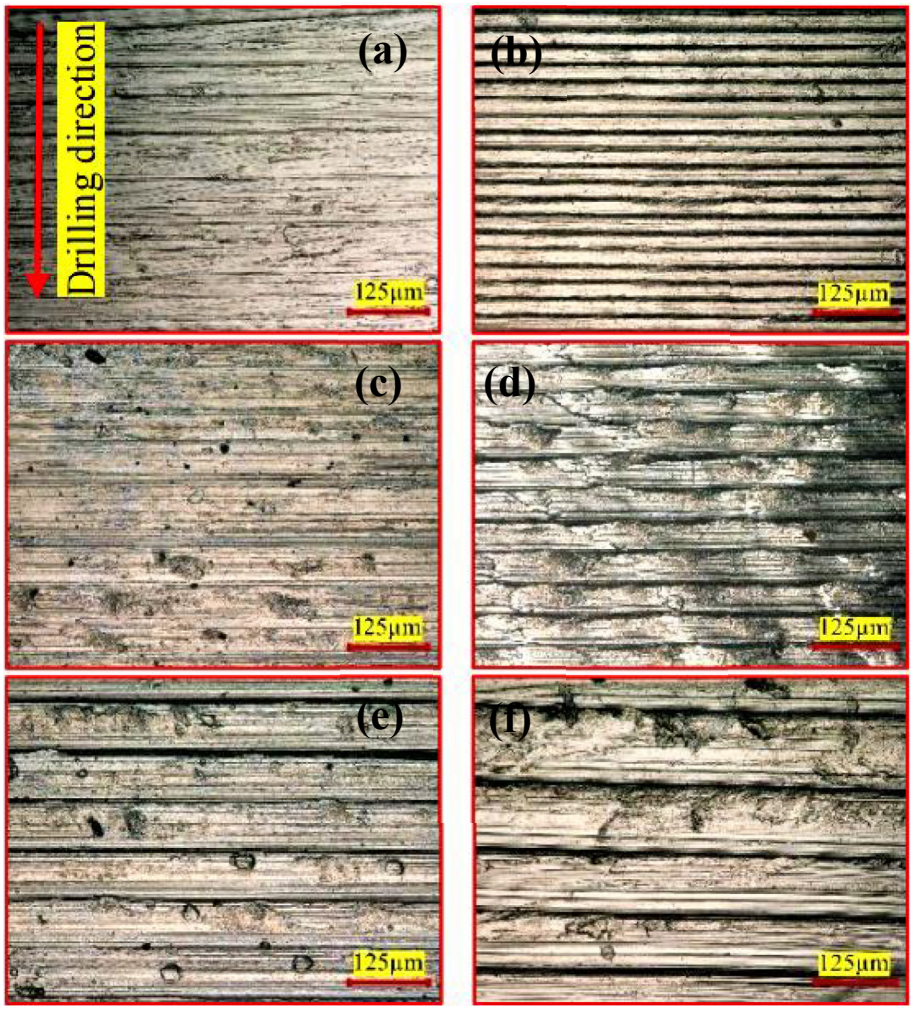

Fig. 19 – Surface topography of SLMed Inconel 718 after drilling at (a) cutting speed 15 m/min of and feed rate of 0.025 mm/rev, (b) cutting speed of 30 m/min and feed rate of 0.025 mm/rev, (c) cutting speed of 15 m/min and feed rate of 0.05 mm/rev, (d) cutting speed of 30 m/min and feed rate of 0.05 mm/rev, (e) cutting speed of 15 m/min and feed rate of and 0.075 mm/rev, (f) cutting speed of 30 m/min and feed rate of 0.075 mm/rev [69].

machining conditions. At the lower temperature, the plasticity of the material was significantly reduced and resulted in grooved and irregular feed marks on the contained surface under cryogenic machining. The number of surface defects increased with increasing feed rate nevertheless the processing route and cooling strategy. The EBM workpiece

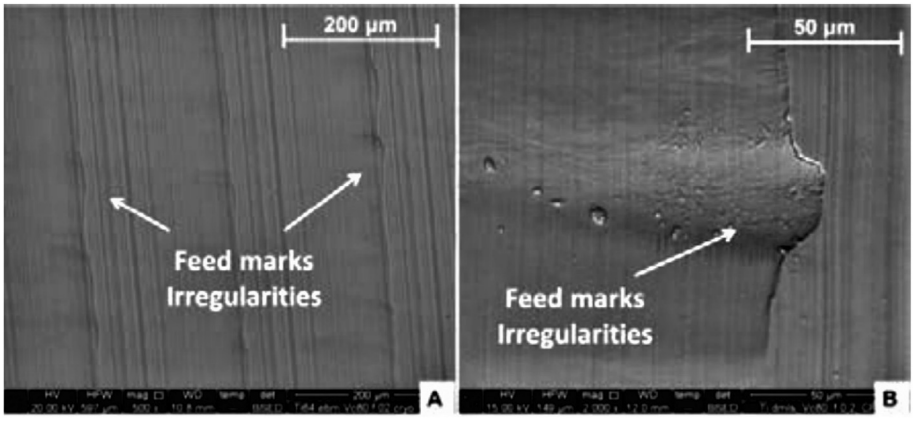

Fig. 20 – The irregularity and feed marks generated during turning of Ti–6Al–4V under cryogenic cooling at (a) 500× magnification and (b) 1000× magnification [76].

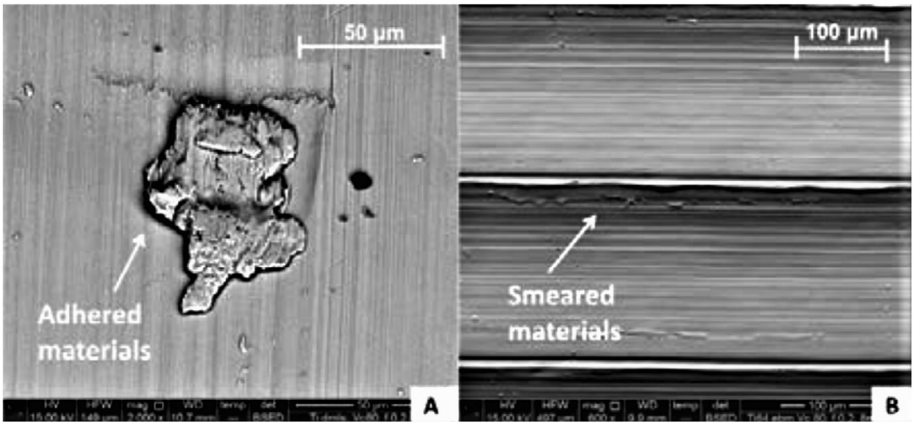

Fig. 21 – Induced surface defects (a) adhered material and (b) smeared material when turning of Ti–6Al–4V under dry cutting [76].

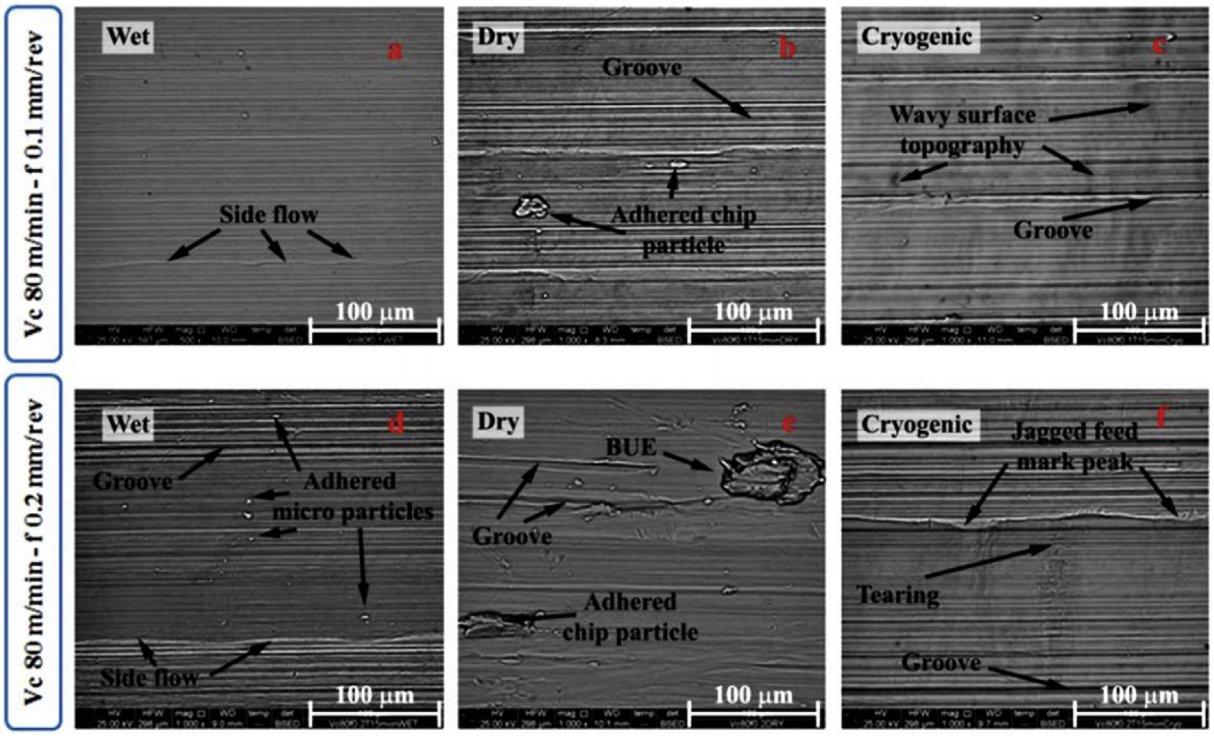

Fig. 22 – Induced surface defects when turning of AMed Ti–6Al–4V under dry, wet and cryogenic cooling [77].

exhibited higher corrosion resistance compared with the wrought workpiece. This was due to the use of cryogenic cooling. In a study of surface characteristics, Bruschi et al. [82] observed that the increment in machined surface microhardness of the wrought titanium was 24% higher than that of EBM titanium under cryogenic cooling. The effect of increasing the feed rate recorded a contrary result, i.e. the higher feed rate produced a smoother surface for the EBM sample under cryogenic cooling while the opposite occurred for the wrought component. The microhardness of the wrought component was significantly affected by the cutting speed under cryogenic cooling. The cooling strategy influenced the residual compressive stresses induced by machining. The cryogenic cooling improved the residual compressive stresses parallel to the axial direction for both wrought and AMed parts. However, the surface roughness was not influenced by the environmental conditions of the machining. The microchemical analysis of the workpiece revealed that a higher quantity of CoCrMo flat plated was adhered to the cryogenically machined workpiece compared with dry turning. Bertolini et al. [84] compared the surface integrity of wrought and AMed Ti–6Al–4V produced by EBM under dry, flood, and cryogenic machining. They found that the machining induced layer from the EBM sample was thicker when compared with the wrought sample. In addition, cryogenic cooling was more effective when compared with

dry and flood machining. The cryogenic cooling provided better residual stresses and nano-hardness; however, the surface integrity of the wrought part was not appreciably affected by the cryogenic machining. The surface integrity of the EBM sample fared the worst of all machining conditions compared with the wrought sample. Compared with the dry and flood machining, fewer particles have adhered to the cryogenically machined surface. However, the lower cutting temperature caused by cryogenic machining lowered the plasticity of the material, which induced grooves followed by irregular feed smears on the machined surface. Lizzul et al. [85] studied the effect of the microstructure caused by AM on the surface integrity of LPBF produced Ti–6Al–4V parts. The size of β grains was affected by the scanning strategy, which had a direct influence on the microhardness of the sample. The microhardness of the sample had a greater impact on the thickness of the highly deformed layer and the hardening of the subsurface strain. The α phase layer and the β grains had a higher impact on the surface roughness. Cryogenic, machining produced a lower surface roughness and improved the impact of the microstructure of AMed manufactured parts on the surface integrity. In another study, Lizzul et al. [93] analyzed the effect of the build direction on the machined surface topography during the milling of AMed Ti–6Al–4V fabricated by LPBF. The sample with 0° (horizontal development of the AM part) showed a higher pick and surface complexity at higher feed/tooth compared with the sample of 90° (vertical development of the AM part). The surface skewness value for the 0° sample was average to positive while it was negative for the sample of 90°. The surface defects and the surface topology were significantly more affected by the cutting parameters than by the build direction. The lower cutting power, followed by the cutting force, was required for the sample of 0° due to the high angle of a shear plane and a lower chip comparison ratio compared with the sample of 90°.

The above analysis confirms that the post-process machining significantly reduced the surface roughness of the final machined component. The feed rate has a greater influence on the surface roughness than does the cutting speed. Furthermore, the AMed porosity induced by AM can be significantly reduced by the processes in finish machining. The AMed processes increase the hardness of the component, which makes it difficult to machine the component and, therefore, the higher hardness results in lower surface roughness. The work hardening effect resulting from the SLM process increases the subsurface and surface hardness, while the partially melted powder material causes surface irregularities following the SLM process. The increasing mechanical and thermal load on the AMed workpiece increased the value of microhardness at a higher feed rate and cutting speed.

7. Conclusions

This review presents a summary of advances that have been made in the field of machining of AMed nickel and titanium-based alloys. AM helps to mitigate the higher overall cost and the variation in material properties at elevated temperatures of the conventionally produced material. Additionally, the machining of the AMed materials is a prerequisite for the provision of an anticipated shape and geometry in specific industrial applications. The followings are the conclusions from this review:

- The optimized set of machining parameters for AMed nickel and/or titanium workpieces is different from those for wrought.
- In some instances, where the hardness of the AMed workpiece was higher than the wrought workpiece, higher cutting forces were observed during machining. In contrast, lower cutting forces were generated when machining high hardness AMed parts. This can be attributed to the differences in the cutting tool geometries used in these studies. However, further research is required to provide greater clarity.
- Where higher cutting forces were generated during machining of AMed parts, correspondingly higher rates of tool wear were also observed. The tool life was shown to be improved when cryogenic coolant and/or MQL coolant were used during machining.
- The cryogenic cooling strategy could significantly lower down the cutting temperature and the wear rate of the cutting tools by reducing crater formation up to 60% for AMed titanium alloys.
- The orientation of the cutting tool concerning the build direction of the printed component had a significant impact on the surface quality of the machined parts which became worse at higher cutting speeds and feed rates.
- The SLMed manufactured titanium alloys have exhibited average of 9–32% of increment in hardness and 3–26% of reduction in cutting force due to different cooling/lubrication strategies used during machining.
- A very poor machined surface finish resulted where the AMed parts had defects, such as pores, unmelted powder particles, microstructural inhomogeneity due to segregation of secondary phase particles.
- The chips formed when machining AMed parts were shorter due to the high hardness and low plastic deformation of the samples.
- Coated cutting tools performed better, reducing the cutting force, chatter, and cutting temperatures when machining the AMed nickel-based workpiece compared with its wrought counterpart.
- The adoption of the adaptive control system could be beneficial in preventing the cutting force variation, which could enhance surface roughness. This system can adjust the controlling parameters according to variations in the microstructure of the material and can generate favorable machining conditions to provide the desired output.

8. Future scope of research

The aforementioned literature reviews exhaustively explained the machining behavior of nickel and titanium-based alloys. The following points have been recognized as potential research directions in the field of machining nickel and titanium-based alloys.

- There is a lack of research studies that investigated the effect of tool coating on the machinability of nickel and titanium-based alloys. In addition, the comparison among the tool coating needs to exemplify during the machining of AMed alloys.
- In-depth surface roughness and tool wear analysis can be done using various lubrication strategies during machining of AMed nickel and titanium-based alloys such as EMQL, nano-MQL, nano-EMQL, Cryo + MQL, and Cryo + EMQL.
- Few studies have been performed on the non-conventional machining operations which need to be further explored.
- Minimal work has been done on the power consumption during the machining of AMed alloys.
- Life cycle analysis of the machining processes with AMed alloys shall open-up new avenues of research in additive-cum-subtractive manufacturing domain.

Declaration of Competing Interest

The authors declare that they have no known competing financial interests or personal relationships that could have appeared to influence the work reported in this paper.

Acknowledgments

The authors are grateful to the Government of Gujarat, India for the funding to establish Advanced Manufacturing lab at IITRAM. The collaborative project work at the lab led to the successful completion of two B.Tech theses.

REFERENCES

[1] Standard ASTM. Standard terminology for additive manufacturing technologies. ASTM International F2792-12a. 2012.
[2] Youssef HA, El-Hofy HA, Ahmed MH. Manufacturing technology: materials, processes, and equipment. CRC Press; 2011.
[3] Guo N, Leu MC. Additive manufacturing: technology, applications and research needs. Front Mech Eng 2013;8(3):215–43.
[4] Gibson I, Rosen D, Stucker B, Khorasani M. Additive manufacturing technologies, vol. 17. New York: Springer; 2014. p. 195. 7.
[5] Wong KV, Hernandez A. A review of additive manufacturing. Int Sch Res Notices 2012;2012.
[6] ASTM International. ISO/ASTM52900-15 standard terminology for additive manufacturing – general principles – terminology. West Conshohocken, PA: ASTM International; 2015.
[7] Yakout M, Elbestawi MA, Veldhuis SC. A review of metal additive manufacturing technologies. SSP 2018;278:1–14.
[8] Waterman NA, Dickens P. Rapid product development in the USA, Europe and Japan. World Class Des Manuf 1994;1(3):27–36.
[9] Jacobs PF. Fundamentals of stereolithography. In: 1992 International Solid Freeform Fabrication Symposium; 1992.
[10] Mireles J, Espalin D, Roberson D, Zinniel B, Medina F, Wicker R. Fused deposition modeling of metals. In: Proceedings of the Solid Freeform Fabrication Symposium, Austin, TX, USA; 2012. p. 6–8. Corpus ID: 26739115.
[11] Kruth JP, Mercelis P, Van Vaerenbergh J, Froyen L, Rombouts M. Binding mechanisms in selective laser sintering and selective laser melting. Rapid Prototyp J 2005;11(1):26–36.
[12] Khanna N, Mistry S, Rashid RR, Gupta MK. Investigations on density and surface roughness characteristics during selective laser sintering of Invar-36 alloy. Mater Res Express 2019;6(8):086541.
[13] Gupta MK, Singla AK, Ji H, Song Q, Liu Z, Cai W, et al. Impact of layer rotation on micro-structure, grain size, surface integrity and mechanical behaviour of SLM Al-Si-10Mg alloy. J Mater Res Technol 2020;9(5):9506–22.
[14] Ponnusamy P, Rahman Rashid RA, Masood SH, Ruan D, Palanisamy S. Mechanical properties of SLM-printed aluminium alloys: a review. Materials 2020;13(19):4301.
[15] Zhang LC, Liu Y, Li S, Hao Y. Additive manufacturing of titanium alloys by electron beam melting: a review. Adv Eng Mater 2018;20(5):1700842.
[16] Rashid RR, Palanisamy S, Attar H, Bermingham M, Dargusch MS. Metallurgical features of direct laser-deposited Ti6Al4V with trace boron. J Manuf Process 2018;35:651–6.
[17] Balla VK, DeVasConCellos PD, Xue W, Bose S, Bandyopadhyay A. Fabrication of compositionally and structurally graded Ti–TiO2 structures using laser engineered net shaping (LENS). Acta Biomater 2009;5(5):1831–7.
[18] Rahman Rashid RA, Barr CJ, Palanisamy S, Nazari KA, Orchowski N, Matthews N, et al. Effect of clad orientation on the mechanical properties of laser-clad repaired ultra-high strength 300 M steel. Surf Coat Technol 2019;380.
[19] Sachs E, Cima M, Cornie J, Brancazio D, Bredt J, Curodeau A, et al. Three-dimensional printing: the physics and implications of additive manufacturing. CIRP Ann 1993;42(1):257–60.
[20] Liao YS, Li HC, Chiu YY. Study of laminated object manufacturing with separately applied heating and pressing. Int J Adv Manuf Technol 2006;27(7–8):703–7.
[21] Bermingham MJ, Thomson-Larkins J, St John DH, Dargusch MS. Sensitivity of Ti-6Al-4V components to oxidation during out of chamber wire + arc additive manufacturing. J Mater Process Technol 2018;258:29–37.
[22] Geng H, Li J, Xiong J, Lin X, Zhang F. Optimization of wire feed for GTAW based additive manufacturing. J Mater Process Technol 2017;243:40–7.
[23] Bermingham MJ, Nicastro L, Kent D, Chen Y, Dargusch MS. Optimising the mechanical properties of Ti-6Al-4V components produced by wire + arc additive manufacturing with post-process heat treatments. J Alloys Compd 2018;753:247–55.
[24] Yang D, He C, Zhang G. Forming characteristics of thin-wall steel parts by double electrode GMAW based additive manufacturing. J Mater Process Technol 2016;227:153–60.
[25] Dhinakaran V, Ajith J, Fahmidha AFY, Jagadeesha T, Sathish T, Stalin B. Wire arc additive manufacturing (WAAM) process of nickel-based superalloys – a review. Mater Today Proc 2020;21:920–5.
[26] Attar H, Bermingham MJ, Ehtemam-Haghighi S, Dehghan-Manshadi A, Kent D, Dargusch MS. Evaluation of the mechanical and wear properties of titanium produced by three different additive manufacturing methods for biomedical application. Mater Sci Eng A 2019;760:339–45.
[27] Mereddy S, Bermingham MJ, Kent D, Dehghan-Manshadi A, StJohn DH, Dargusch MS. Trace carbon addition to refine

microstructure and enhance properties of additive-manufactured Ti-6Al-4V. JOM 2018;70(9):1670–6.
[28] MELD Manufacturing. http://meldmanufacturing.com/; 2020.
[29] Klocke F, Roderburg A, Zeppenfeld C. Design methodology for hybrid production processes. Procedia Eng 2011;9:417–30.
[30] Nau B, Roderburg A, Klocke F. Ramp-up of hybrid manufacturing technologies. CIRP J Manuf Sci Technol 2011;4(3):313–6.
[31] Zhumatay N, Perveen A. Hybrid machining process for microfabrication of micro parts. Mater Today Proc 2019;18:2209–16.
[32] Bambach M, Sizova I, Sydow B, Hemes S, Meiners F. Hybrid manufacturing of components from Ti-6Al-4V by metal forming and wire-arc additive manufacturing. J Mater Process Technol 2020;282:116689.
[33] Liu R, Wang Z, Sparks T, Liou F, Newkirk J. Aerospace applications of laser additive manufacturing. In: Laser additive manufacturing. Woodhead Publishing; 2017. p. 351–71.
[34] Chen S, Murphy J, Herlehy J, Bourell DL, Wood KL. Development of SLS fuel cell current collectors. Rapid Prototyp J 2006;12(5):275–82.
[35] Vafadar A, Guzzomi F, Rassau A, Hayward K. Advances in metal additive manufacturing: a review of common processes, industrial applications, and current challenges. Appl Sci 2021;11(3):1213.
[36] Kent D, Rahman Rashid R, Bermingham M, Attar H, Sun S, Dargusch M. Insights into machining of a β titanium biomedical alloy from chip microstructures. Metals 2018;8(9):710.
[37] Dhariwala B, Hunt E, Boland T. Rapid prototyping of tissue-engineering constructs, using photopolymerizable hydrogels and stereolithography. Tissue Eng 2004;10(9–10):1316–22.
[38] Ivanova O, Williams C, Campbell T. Additive manufacturing (AM) and nanotechnology: promises and challenges. Rapid Prototyp J 2013;19(5):353–64.
[39] Cooper D, Thornby J, Blundell N, Henrys R, Williams MA, Gibbons G. Design and manufacture of high-performance hollow engine valves by additive layer manufacturing. Mater Des 2015;69:44–55.
[40] Leal R, Barreiros FM, Alves L, Romeiro F, Vasco JC, Santos M, et al. Additive manufacturing tooling for the automotive industry. Int J Adv Manuf Technol 2017;92(5):1671–6.
[41] Ma D, Stoica AD, Wang Z, Beese AM. Crystallographic texture in an additively manufactured nickel-base superalloy. Mater Sci Eng A 2017;684:47–53.
[42] Komarasamy M, Shukla S, Williams S, Kandasamy K, Kelly S, Mishra RS. Microstructure, fatigue, and impact toughness properties of additively manufactured nickel alloy 718. Addit Manuf 2019;28:661–75.
[43] Solberg K, Berto F. Notch-defect interaction in additively manufactured Inconel 718. Int J Fatigue 2019;122:35–45.
[44] Khanna N, Shah P, Agrawal C, Pusavec F, Hegab H. Inconel 718 machining performance evaluation using indigenously developed hybrid machining facilities: experimental investigation and sustainability assessment. Int J Adv Manuf Technol 2020;106(11):4987–99.
[45] Chan KS. Mechanism-based models for predicting the microstructure and stress–strain response of additively manufactured superalloy 718Plus. J Mater Eng Perform 2020:1–11.
[46] Dubiel B, Sieniawski J. Precipitates in additively manufactured Inconel 625 superalloy. Materials 2019;12(7):1144.
[47] Bermingham MJ, McDonald SD, Dargusch MS. Effect of trace lanthanum hexaboride and boron additions on microstructure, tensile properties and anisotropy of Ti-6Al-4V produced by additive manufacturing. Mater Sci Eng A 2018;719:1–11.
[48] Liu S, Shin YC. Additive manufacturing of Ti6Al4V alloy: a review. Mater Des 2019;164:107552.
[49] Singla AK, Banerjee M, Sharma A, Singh J, Bansal A, Gupta MK, et al. Selective laser melting of Ti6Al4V alloy: process parameters, defects and post-treatments. J Manuf Process 2021;64:161–87.
[50] Zhang J, Wang X, Paddea S, Zhang X. Fatigue crack propagation behaviour in wire + arc additive manufactured Ti-6Al-4V: effects of microstructure and residual stress. Mater Des 2016;90:551–61. https://doi.org/10.1016/j.matdes.2015.10.141.
[51] Khanna N, Rashid RR, Palanisamy S. Experimental evaluation of the effect of workpiece heat treatments and cutting parameters on the machinability of Ti-10V-2Fe-3Al β titanium alloy using Taguchi's design of experiments. Int J Mach Mach Mater 2017;19(4):374–93.
[52] Chen L, Xu Q, Liu Y, Cai G, Liu J. Machinability of the laser additively manufactured Inconel 718 superalloy in turning. Int J Adv Manuf Technol 2021;114(3):871–82.
[53] Careri F, Umbrello D, Essa K, Attallah MM, Imbrogno S. The effect of the heat treatments on the tool wear of hybrid additive manufacturing of IN718. Wear 2021;470:203617.
[54] Kaynak Y, Tascioglu E. Post-processing effects on the surface characteristics of Inconel 718 alloy fabricated by selective laser melting additive manufacturing. Prog Addit Manuf 2020;5(2):221–34.
[55] Kaynak Y, Tascioglu E. Finish machining-induced surface roughness, microhardness and XRD analysis of selective laser melted Inconel 718 alloy. Procedia CIRP 2018;71:500–4.
[56] Calleja A, Urbikain G, González H, Cerrillo I, Polvorosa R, Lamikiz A. Inconel® 718 superalloy machinability evaluation after laser cladding additive manufacturing process. Int J Adv Manuf Technol 2018;97(5):2873–85.
[57] Yang L, Patel KV, Jarosz K, Özel T. Surface integrity induced in machining additively fabricated nickel alloy Inconel 625. Procedia CIRP 2020;87:351–4.
[58] Jarosz K, Patel KV, Özel T. Mechanistic force modeling in finish face milling of additively manufactured Inconel 625 nickel-based alloy. Int J Adv Manuf Technol 2020;111(5):1535–51.
[59] Sen C, Subasi L, Ozaner OC, Orhangul A. The effect of milling parameters on surface properties of additively manufactured Inconel 939. Procedia CIRP 2020;87:31–4.
[60] Fei J, Liu G, Patel K, Özel T. Effects of machining parameters on finishing additively manufactured nickel-based alloy Inconel 625. J Manuf Mater Process 2020;4(2):32.
[61] Fei J, Liu G, Patel K, Özel T. Cutting force investigation in face milling of additively fabricated nickel alloy 625 via powder bed fusion. Int J Mechatron Manuf Syst 2019;12(3–4):196–210.
[62] Periane S, Duchosal A, Vaudreuil S, Chibane H, Morandeau A, Xavior MA, et al. Selection of machining condition on surface integrity of additive and conventional Inconel 718. Procedia CIRP 2020;87:333–8.
[63] Tascioglu E, Kaynak Y, Poyraz Ö, Orhangül A, Ören S. The effect of finish-milling operation on surface quality and wear resistance of Inconel 625 produced by selective laser melting additive manufacturing. In: International conference on advanced surface enhancement. Singapore: Springer; 2019. p. 263–72.
[64] Ostra T, Alonso U, Veiga F, Ortiz M, Ramiro P, Alberdi A. Analysis of the machining process of inconel 718 parts

manufactured by laser metal deposition. Materials 2019;12(13):2159.
[65] Ji H, Gupta MK, Song Q, Cai W, Zheng T, Zhao Y, et al. Microstructure and machinability evaluation in micro milling of selective laser melted Inconel 718 alloy. J Mater Res Technol 2021;14:348–62.
[66] Park E, Kim DM, Park HW, Park YB, Kim N. Evaluation of tool life in the dry machining of Inconel 718 parts from additive manufacturing (AM). Int J Precis Eng Manuf 2020;21(1):57–65.
[67] Sadiq MA, Hoang NM, Valencia N, Obeidat S, Hung WN. Experimental study of micromilling selective laser melted Inconel 718 superalloy. Procedia Manuf 2018;26:983–92.
[68] Periane S, Duchosal A, Vaudreuil S, Chibane H, Morandeau A, Cormier J, et al. Machining influence on the fatigue resistance of Inconel 718 fabricated by selective laser melting (SLM). Procedia Struct Integr 2019;19:415–22.
[69] Karabulut Y, Kaynak Y. Drilling process and resulting surface properties of Inconel 718 alloy fabricated by selective laser melting additive manufacturing. Procedia CIRP 2020;87:355–9.
[70] Lynch ME, Williams K, Cabrera M, Beccuti T. Surface finishing of additively manufactured IN718 lattices by electrochemical machining. Int J Adv Manuf Technol 2021;113(3):967–84.
[71] Ozaner OC, Dursun G, Akbulut G. Effects of wire-EDM parameters on the surface integrity and mechanical characteristics of additively manufactured Inconel 939. Mater Today Proc 2021;38:1861–5.
[72] Polishetty A, Shunmugavel M, Goldberg M, Littlefair G, Singh RK. Cutting force and surface finish analysis of machining additive manufactured titanium alloy Ti-6Al-4V. Procedia Manuf 2017;7:284–9.
[73] Sartori S, Bordin A, Moro L, Ghiotti A, Bruschi S. The influence of material properties on the tool crater wear when machining Ti6Al4V produced by additive manufacturing technologies. Procedia CIRP 2016;46:587–90.
[74] Sartori S, Moro L, Ghiotti A, Bruschi S. On the tool wear mechanisms in dry and cryogenic turning additive manufactured titanium alloys. Tribol Int 2017;105:264–73.
[75] Oyelola O, Crawforth P, M'Saoubi R, Clare AT. Machining of additively manufactured parts: implications for surface integrity. Procedia CIRP 2016;45:119–22.
[76] Sartori S, Bordin A, Ghiotti A, Bruschi S. Analysis of the surface integrity in cryogenic turning of Ti6Al4 v produced by direct melting laser sintering. Procedia CIRP 2016;45:123–6.
[77] Bordin A, Sartori S, Bruschi S, Ghiotti A. Experimental investigation on the feasibility of dry and cryogenic machining as sustainable strategies when turning Ti6Al4V produced by additive manufacturing. J Clean Prod 2017;142:4142–51.
[78] Bordin A, Bruschi S, Ghiotti A, Bariani PF. Analysis of tool wear in cryogenic machining of additive manufactured Ti6Al4V alloy. Wear 2015;328:89–99.
[79] Bordin A, Bruschi S, Ghiotti A, Bucciotti F, Facchini L. Comparison between wrought and EBM Ti6Al4V machinability characteristics. In: Key engineering materials, vol. 611. Trans Tech Publications Ltd; 2014. p. 1186–93.
[80] Bertolini R, Lizzul L, Pezzato L, Ghiotti A, Bruschi S. Improving surface integrity and corrosion resistance of additive manufactured Ti6Al4V alloy by cryogenic machining. Int J Adv Manuf Technol 2019;104(5):2839–50.
[81] Oyelola O, Crawforth P, M'Saoubi R, Clare AT. Machining of functionally graded Ti6Al4V/WC produced by directed energy deposition. Addit Manuf 2018;24:20–9.
[82] Bruschi S, Bertolini R, Bordin A, Medea F, Ghiotti A. Influence of the machining parameters and cooling strategies on the wear behavior of wrought and additive manufactured Ti6Al4V for biomedical applications. Tribol Int 2016;102:133–42.
[83] Le Coz G, Fischer M, Piquard R, D'Acunto A, Laheurte P, Dudzinski D. Micro cutting of Ti-6Al-4V parts produced by SLM process. Procedia CIRP 2017;58:228–32.
[84] Bertolini R, Lizzul L, Bruschi S, Ghiotti A. On the surface integrity of Electron Beam Melted Ti6Al4V after machining. Procedia CIRP 2019;82:326–31.
[85] Lizzul L, Bertolini R, Ghiotti A, Bruschi S. Effect of AM-induced anisotropy on the surface integrity of laser powder bed fused Ti6Al4V machined parts. Procedia Manuf 2020;47:505–10.
[86] Bordin A, Imbrogno S, Rotella G, Bruschi S, Ghiotti A, Umbrello D. Finite element simulation of semi-finishing turning of electron beam melted Ti6Al4V under dry and cryogenic cooling. Procedia CIRP 2015;31:551–6.
[87] Huang X, Bai Q, Li YT, Zhang B. Machining finish of titanium alloy prepared by additive manufacturing. In: Applied mechanics and materials, vol. 872. Trans Tech Publications Ltd; 2017. p. 43–8.
[88] Veiga F, Gil Del Val A, Suárez A, Alonso U. Analysis of the machining process of titanium Ti6Al-4V parts manufactured by wire arc additive manufacturing (WAAM). Materials 2020;13(3):766.
[89] Bonaiti G, Parenti P, Annoni M, Kapoor S. Micro-milling machinability of DED additive titanium Ti-6Al-4V. Procedia Manuf 2017;10:497–509.
[90] Moritz J, Seidel A, Kopper M, Bretschneider J, Gumpinger J, Finaske T, et al. Hybrid manufacturing of titanium Ti-6Al-4V combining laser metal deposition and cryogenic milling. Int J Adv Manuf Technol 2020;107(7):2995–3009.
[91] Lizzul L, Sorgato M, Bertolini R, Ghiotti A, Bruschi S. Influence of additive manufacturing-induced anisotropy on tool wear in end milling of Ti6Al4V. Tribol Int 2020;146:106200.
[92] Hojati F, Daneshi A, Soltani B, Azarhoushang B, Biermann D. Study on machinability of additively manufactured and conventional titanium alloys in micro-milling process. Precis Eng 2020;62:1–9.
[93] Lizzul L, Sorgato M, Bertolini R, Ghiotti A, Bruschi S. Anisotropy effect of additively manufactured Ti6Al4V titanium alloy on surface quality after milling. Precis Eng 2021;67:301–10.
[94] Khaliq W, Zhang C, Jamil M, Khan AM. Tool wear, surface quality, and residual stresses analysis of micro-machined additive manufactured Ti–6Al–4V under dry and MQL conditions. Tribol Int 2020;151:106408.
[95] Li S, Zhang B, Bai Q. Effect of temperature buildup on milling forces in additive/subtractive hybrid manufacturing of Ti-6Al-4V. Int J Adv Manuf Technol 2020;107(9):4191–200.
[96] de Oliveira Campos F, Araujo AC, Munhoz ALJ, Kapoor SG. The influence of additive manufacturing on the micromilling machinability of Ti6Al4V: a comparison of SLM and commercial workpieces. J Manuf Process 2020;60:299–307.
[97] Zhang H, Dang J, Ming W, Xu X, Chen M, An Q. Cutting responses of additive manufactured Ti6Al4V with solid ceramic tool under dry high-speed milling processes. Ceram Int 2020;46(10):14536–47.

[98] Gong X, Manogharan G. Machining behavior and material properties in additive manufacturing Ti-6Al-4V parts. In: International manufacturing science and engineering conference, vol. 84256. American Society of Mechanical Engineers (ASME); 2020. p. V001T01A055.
[99] Oyelola O, Jackson-Crisp A, Crawforth P, Pieris DM, Smith RJ, M'Saoubi R, et al. Machining of directed energy deposited Ti6Al4V using adaptive control. J Manuf Process 2020;54:240–50.
[100] Hoye N, Cuiuri D, Rashid RR, Palanisamy S. Machining of GTAW additively manufactured Ti-6Al-4V structures. Int J Adv Manuf Technol 2018;99(1):313–26.
[101] Rysava Z, Bruschi S, Carmignato S, Medeossi F, Savio E, Zanini F. Micro-drilling and threading of the Ti6Al4 v titanium alloy produced through additive manufacturing. Procedia CIRP 2016;46:583–6.
[102] Alonso U, Veiga F, Suárez A, Artaza T. Experimental investigation of the influence of wire arc additive manufacturing on the machinability of titanium parts. Metals 2020;10(1):24.
[103] Dang J, Liu G, Chen Y, An Q, Ming W, Chen M. Experimental investigation on machinability of DMLS Ti6Al4V under dry drilling process. Mater Manuf Process 2019;34(7):749–58.
[104] Ming W, Dang J, An Q, Chen M. Chip formation and hole quality in dry drilling additive manufactured Ti6Al4V. Mater Manuf Process 2020;35(1):43–51.
[105] Woo WS, Kim EJ, Jeong HI, Lee CM. Laser-assisted machining of Ti-6Al-4V fabricated by DED additive manufacturing. Int J Precis Eng Manuf Green Technol 2020;7(3):559–72.

Dr. Navneet Khanna is an Associate Dean (Career Development and Promotion of Innovation and Industrial Research) and former Mechanical Engineering department coordinator at IITRAM. He worked as Assistant Professor at BITS Pilani, Pilani campus and also taught at IIT Gandhinagar as an adjunct faculty. He is a specialist in building strong pool of trained engineering graduates and involved in solving Manufacturing related problems of Indian Industries and Government Organizations. He bagged Early Career Research Award of SERB (Government of India) and successfully completed the project. He has successfully led 70+ projects defined by the Indian industries and published 50+ research papers in renowned (SCI/SCIE) peer-reviewed journals. In addition to this core competence, he has created several avenues of collaborative work with ISRO, DRDO, IPR, IITs and renowned institutions in USA, AUSTRALIA, UK, FRANCE, SLOVENIA, POLAND etc …

Kishan Zadafiya, recently graduated student from the Institute of Infrastructure Technology Research and Management (IITRAM), Ahmedabad. As an undergraduate student, he was actively researching to identify the impact of sustainable cutting fluid strategies like Minimum Quantity Lubrication (MQL), Electrostatic MQL (EMQL), and nano-particles immersed EMQL. He has also published two research papers in Tribology International and Journal of manufacturing processes. Shah P, Khanna N, **Zadafiya K**, Bhalodiya M, Maruda RW, Krolczyk GM. In-house development of eco-friendly lubrication techniques (EMQL, Nanoparticles + EMQL, and EL) for improving machining performance of 15–5 PHSS. Tribology International 2020:106476. **Zadafiya K**, Shah P, Shokrani A, Khanna N. Recent advancements in nano-lubrication strategies for machining processes considering their health and environmental impacts. Journal of Manufacturing Processes. 2021 Aug 1; 68:481–511.

Tej Patel, recently graduated student from the Institute of Infrastructure Technology Research and Management (IITRAM), Ahmedabad. As an undergraduate student, he was actively indulged in the research of sustainable metal cutting techniques such as ultrasonic-assisted turning and cryogenic machining. He has published two research papers in materials today: proceedings and the International Journal of Advanced Manufacturing Technology. He has recently joined the University of Windsor, Canada as a graduate student in the MEng Industrial Engineering program. **Patel T**, Khanna N, Yadav S, Shah P, Sarikaya M, Singh D, Gupta MK, Kotkunde N. Machinability analysis of nickel-based superalloy Nimonic 90: a comparison between wet and LCO 2 as a cryogenic coolant. The International Journal of Advanced Manufacturing Technology. 2021 Apr; 113(11):3613–28. **Patel T**, Yadav S, Raj Z, Shah P, Khanna N. Analysis of machining performance of AISI 420 stainless steel using conventional and ultrasonic-assisted turning. Materials Today: Proceedings. 2020 Jan 1; 26:2200–7.

Dr. Yusuf Kaynak is a Professor of Mechanical Engineering at Marmara University, Istanbul, Turkey. He received his Ph.D. in Mechanical Engineering from the University of Kentucky, USA in 2013. His research interest includes machining, additive manufacturing, post processing and surface integrity.

Dr. Rizwan Abdul Rahman Rashid completed his PhD from The University of Queensland in 2013. His work was on the laser-assisted machining of beta titanium alloys. Since then, he is working as a Post-doctoral Research Fellow at Swinburne University of Technology. He is also working with Defence Materials Technology Centre (DMTC) for the past 10 years on a number of projects, including New Manufacturing Capability, Enhanced Tooling Capability, Sustainment Capability Development and Benchmarking for Best Practices. In his work with DMTC, Dr. Rahman Rashid has engaged in research activities with other DMTC industry partners such as RUAG, Seco Tools, and Sutton Tools. His work involved research activities in advanced manufacturing and repair technologies, machining of hard-to-machine materials and laser ultrasonic non-destructive testing at Swinburne. He has also engaged in welding benchmarking of maritime-grade steels with SMEs across Australia and New Zealand.

Dr. Ana Vafadar was awarded a Ph.D. in Mechanical Engineering from Australia, and her Ph.D. research was focused on developing economic and technical frameworks for advanced manufacturing systems. She is a lecturer at Edith Cowan University (ECU), currently lecturing in engineering courses and project-based units as well as coordinating the Fabrocation and Prototyping Makerspace labs at ECU. She is an active academic and researcher in Mechanical and Manufacturing Engineering disciplines with keen interests in advanced manufacturing systems, additive manufacturing (3D printing), optimization, materials and mechanical design (e.g., design of high efficiency, and novel heat exchangers).